

1                   **LegacyClimate 1.0: A dataset of pollen-based climate**  
2                   **reconstructions from 2594 Northern Hemisphere sites covering the**  
3                   **last 30 ka and beyond**

4                   Ulrike Herzschuh<sup>1,2,3</sup>, Thomas Böhmer<sup>1</sup>, Chenzhi Li<sup>1,2</sup>, Manuel Chevalier<sup>4,5</sup>, Raphaël Hébert<sup>1</sup>, Anne  
5                   Dallmeyer<sup>6</sup>, Xianyong Cao<sup>1,7</sup>, Nancy H. Bigelow<sup>8</sup>, Larisa Nazarova<sup>1,9</sup>, Elena Y. Novenko<sup>10,11</sup>, Jungjae  
6                   Park<sup>12,13</sup>, Odile Peyron<sup>14</sup>, Natalia A. Rudaya<sup>15,16</sup>, Frank Schlütz<sup>17,18</sup>, Lyudmila S. Shumilovskikh<sup>18</sup>,  
7                   Pavel E. Tarasov<sup>19</sup>, Yongbo Wang<sup>20</sup>, Ruilin Wen<sup>21,22</sup>, Qinghai Xu<sup>23</sup>, Zhuo Zheng<sup>24,25</sup>

8                   <sup>1</sup> Polar Terrestrial Environmental Systems, Alfred Wegener Institute Helmholtz Centre for Polar and  
9                   Marine Research, Telegrafenberg A45, 14473 Potsdam, Germany

10                  <sup>2</sup> Institute of Environmental Science and Geography, University of Potsdam, Karl-Liebknecht-Str. 24-  
11                  25, 14476 Potsdam, Germany

12                  <sup>3</sup> Institute of Biochemistry and Biology, University of Potsdam, Karl-Liebknecht-Str. 24-25, 14476  
13                  Potsdam, Germany

14                  <sup>4</sup> Institute of Geosciences, Sect. Meteorology, Rheinische Friedrich-Wilhelms-Universität Bonn, Auf  
15                  dem Hügel 20, 53121 Bonn, Germany

16                  <sup>5</sup> Institute of Earth Surface Dynamics IDYST, Faculté des Géosciences et l'Environnement, University  
17                  of Lausanne, Bâtiment Géopolis, 1015 Lausanne, Switzerland

18                  <sup>6</sup> Max Planck Institute for Meteorology, Bundesstrasse 53, 20146 Hamburg, Germany

19                  <sup>7</sup> Alpine Paleoecology and Human Adaptation Group (ALPHA), State Key Laboratory of Tibetan  
20                  Plateau Earth System, and Resources and Environment (TPESRE), Institute of Tibetan Plateau  
21                  Research, Chinese Academy of Sciences, 100101 Beijing, China

22                  <sup>8</sup> Alaska Quaternary Center, University of Alaska Fairbanks, Fairbanks, Alaska 99775, USA

23                  <sup>9</sup> Kazan Federal University, Kremlyovskaya str. 18, 420008 Kazan, Russia

- 24 <sup>10</sup> Lomonosov Moscow State University, Faculty of geography, Leniskie gory 1, 119991 Moscow,  
25 Russia
- 26 <sup>11</sup> Department of Quaternary Paleogeography, Institute of Geography Russian Academy of Science,  
27 Staromonrtny lane, 29, 119017, Moscow, Russia
- 28 <sup>12</sup> Department of Geography, Seoul National University, 1 Gwanak-ro, Gwanak-gu, Seoul, 08826,  
29 Republic of Korea
- 30 <sup>13</sup> Institute for Korean Regional Studies, Seoul National University, 1 Gwanak-ro, Gwanak-gu, Seoul,  
31 08826, Republic of Korea
- 32 <sup>14</sup> Institut des Sciences de l'Evolution de Montpellier, Université de Montpellier, CNRS UMR 5554,  
33 Montpellier, France
- 34 <sup>15</sup> PaleoData Lab, Institute of Archaeology and Ethnography, Siberian Branch, Russian Academy of  
35 Sciences, Pr. Akademika 36 Lavrentieva 17, 630090 Novosibirsk, Russia
- 36 <sup>16</sup> Biological Institute, Tomsk State University, Pr. Lenina, 26, Tomsk, 634050, Russia
- 37 <sup>17</sup> Lower Saxony Institute for Historical Coastal Research, D-26382 Wilhelmshaven, Germany
- 38 <sup>18</sup> Department of Palynology and Climate Dynamics, Albrecht-von-Haller Institute for Plant Sciences,  
39 University of Göttingen, Untere Karspüle 2, 37073 Göttingen, Germany
- 40 <sup>19</sup> Freie Universität Berlin, Institute of Geological Sciences, Palaeontology Section, Malteserstrasse  
41 74-100, Building D, 12249 Berlin, Germany
- 42 <sup>20</sup> College of Resource Environment and Tourism, Capital Normal University, 105 West 3rd Ring Rd N,  
43 100048 Beijing, China
- 44 <sup>21</sup> Key Laboratory of Cenozoic Geology and Environment, Institute of Geology and Geophysics,  
45 Chinese Academy of Sciences, 19 Beitucheng West Road, Chaoyang District, 100029 Beijing, China
- 46 <sup>22</sup> CAS Center for Excellence in Life and Paleoenvironment, 100044 Beijing, China
- 47 <sup>23</sup> School of Geographic Sciences, Hebei Normal University, 050024 Shijiazhuang, China

48 <sup>24</sup> Guangdong Key Lab of Geodynamics and Geohazards, School of Earth Sciences and Engineering,  
49 Sun Yat-sen University, 519082 Zhuhai, China

50 <sup>25</sup> Southern Marine Science and Engineering Guangdong Laboratory (Zhuhai), 519082 Zhuhai, China

51 **Correspondence:** Ulrike Herzschuh (Ulrike.Herzschuh@awi.de)

52

53 **Abstract.** Here we describe the LegacyClimate 1.0, a dataset of the reconstruction of mean July  
54 temperature ( $T_{\text{July}}$ ), mean annual temperature ( $T_{\text{ann}}$ ), and annual precipitation ( $P_{\text{ann}}$ ) from 2594 fossil  
55 pollen records from the Northern Hemisphere spanning the entire Holocene with some records reaching  
56 back to the Last Glacial. Two reconstruction methods, the Modern Analogue Technique (MAT) and  
57 Weighted-Averaging Partial-Least Squares regression (WA-PLS) reveal similar results regarding spatial  
58 and temporal patterns. To reduce the impact of precipitation on temperature reconstruction and vice  
59 versa, we also provide reconstructions using tailored modern pollen data limiting the range of the  
60 corresponding other climate variables. We assess the reliability of the reconstructions using information  
61 from the spatial distributions of the root-mean-squared error of prediction and reconstruction significance  
62 tests. The dataset is beneficial for synthesis studies of proxy-based reconstructions and to evaluate the  
63 output of climate models and thus help to improve the models themselves. We provide our compilation  
64 of reconstructed  $T_{\text{July}}$ ,  $T_{\text{ann}}$ , and  $P_{\text{ann}}$  as open-access datasets at PANGAEA  
65 (<https://doi.pangaea.de/10.1594/PANGAEA.930512>; Herzschuh et al., 2021). R code for the  
66 reconstructions is provided at Zenodo (<https://doi.org/10.5281/zenodo.5910989>; Herzschuh et al.,  
67 2022b), including harmonized open-access modern and fossil datasets used for the reconstructions, so  
68 that customized reconstructions can be easily established.

69

## 70 **1 Introduction**

71 The comparison of climate model outputs with climate data is essential for model improvements (Eyring  
72 et al., 2019). The extratropical Northern Hemisphere is of particular interest because it is known for  
73 complex spatial and temporal temperature and precipitation patterns. However, the period for which  
74 instrumental observations are available is only of limited use to validate simulations, in particular when  
75 assessing climate response to natural climate drivers because it is too short and because it is impacted

76 by human-induced greenhouse gas forcing. Climate proxy data derived from natural archives are  
77 therefore of great value.

78 Previous proxy-based climate inferences have contributed to major debates about Holocene climate  
79 change. For example, while simulations indicate gradual warming of the Holocene, temperature proxy  
80 data syntheses rather support a mid-Holocene optimum which resulted in the “Holocene conundrum”  
81 debate (Liu et al., 2014). While the debate has progressed since new proxy-based syntheses can help  
82 to understand regional differences and contribute further to the debate. Qualitative proxy-based  
83 inferences indicate that the mid-Holocene in the Northern Hemisphere mid-latitudes was rather dry and  
84 warm compared with present-day in agreement with modeling outputs (Routson et al., 2019). Also,  
85 quantitative precipitation reconstructions from Eastern and Central Asia unveiled the complex monsoon-  
86 westerlies interactions (Chen et al., 2019; Herzschuh et al., 2019). However, evaluating modeling  
87 outputs using proxy-based reconstructions is a complex task and strongly depend on the purpose of the  
88 proxy data-model comparison study (e.g. the purpose of an evaluation could either target the mean or  
89 site-specific changes, or it could target relative changes or absolute values, or the purpose could be to  
90 infer spatial or temporal climate variability at specific scales, etc.). All these types of evaluation require  
91 a specific handling of the proxy-data and have to be considered for proxy-model comparisons.

92 Fossil pollen records are well-established in their use as a palaeoecological and palaeoclimatological  
93 proxy and of great value as indicators of past environmental and climatic change for many decades.  
94 Considerable efforts have been made to establish regional, continental and even global data repositories  
95 like the North American Pollen Database (NAPD; <https://www.ncei.noaa.gov/products/paleoclimatology>,  
96 last access: 1 July 2020), the European Pollen Database (EPD;  
97 <http://www.europeanpollendatabase.net/index.php>, last access: 1 July 2020) and the Neotoma  
98 Paleocology Database (<https://www.neotomadb.org/>, last access: 1 April 2021; Williams et al., 2018).  
99 Pollen data from archives across multiple environmental settings such as lakes, wetlands, or marine  
100 sediments, have been widely used to quantitatively reconstruct past vegetation and climate variables  
101 (Birks, 2019; Chevalier et al., 2020). Among land-derived proxy data, pollen are particularly suitable for  
102 temporarily and spatially high-resolution evaluation of climate model simulations of the late Quaternary  
103 period. A number of methods have been proposed for making pollen-based climate reconstructions  
104 (Chevalier et al., 2020): among them, classification approaches like the Modern Analogue Technique  
105 (MAT) or regression approaches like Weighted-Averaging Partial-Least Squares regression (WA-PLS)  
106 are most commonly used. MAT and WA-PLS rely on extensive collections of modern spectra. Hence,

107 designing a robust calibration dataset from modern pollen assemblages is a crucial part of the  
108 reconstruction process. A suitable calibration dataset should cover a wide range of climatic and  
109 environmental gradients in order to represent an empirical relationship between pollen assemblages  
110 and climate (Birks et al., 2010; Chevalier et al., 2020). Like with fossil pollen records, data syntheses  
111 and repositories also exist for modern surface pollen data e.g. for North America (Whitmore et al., 2005),  
112 Eurasia (Davis et al., 2013 and 2020) and China (Cao et al., 2013; Herzschuh et al., 2019).

113 For temperature reconstruction time-series, several broad-scale syntheses exist; however, either they  
114 originate from different proxies (Kaufman et al., 2020a and 2020b) or are restricted to certain continents  
115 or regions or/and are poorly documented (Mauri et al., 2015; Marsicek et al., 2018; Routson et al., 2019).  
116 Temperature reconstructions from extratropical Asia are mostly lacking. Precipitation syntheses are  
117 available from Europe (Mauri et al., 2015), North America (Gajewski, 2000) and China and Mongolia  
118 (Herzschuh et al., 2019) but, hitherto, no global or hemispheric syntheses of quantitative precipitation  
119 changes are available for the Holocene.

120 In a recent effort, we synthesized and taxonomically harmonized pollen records available in the Neotoma  
121 Paleocology Database (Williams et al., 2018) and additional records from China and Siberia (Cao et  
122 al., 2013 and 2020) into a global Late Quaternary fossil pollen dataset (LegacyPollen 1.0; Herzschuh et  
123 al., 2022c) and revised all chronologies of those records using a Bayesian approach that allows for the  
124 inference of temporal uncertainties (LegacyAge 1.0; Li et al., 2022). Here, in the third part of a series of  
125 interconnected studies, we present the pollen-based reconstruction of mean July temperature ( $T_{\text{July}}$ ),  
126 mean annual temperature ( $T_{\text{ann}}$ ) and annual precipitation ( $P_{\text{ann}}$ ) including reconstruction and temporal  
127 uncertainties as well as quality measures from 2594 records from the Northern Hemisphere using WA-  
128 PLS and MAT (LegacyClimate 1.0; this study).

129

## 130 **2 Methods**

### 131 **2.1 Input data**

132 The objective of this study is to create a dataset of quantitative reconstructions of  $T_{\text{July}}$ ,  $T_{\text{ann}}$  and  $P_{\text{ann}}$   
133 spanning the last 30 ka and beyond from fossil pollen records. These variables (or variables highly  
134 correlated to them) were shown to explain most variance in the modern pollen data ( $T_{\text{July}}$ ,  $P_{\text{ann}}$ ) or are  
135 typically used in syntheses and proxy-model comparison studies ( $T_{\text{ann}}$ ). Accordingly, we selected these

136 three variables. We used the fossil data set compiled in LegacyPollen 1.0 (stored on the PANGAEA  
137 open data repository and presented in Herzschuh et al., 2022c) that integrates pollen records archived  
138 in the Neotoma Paleoecology Database, a dataset from Eastern and Central Asia (Cao et al., 2013;  
139 Herzschuh et al., 2019) and a dataset from Northern Asia (Cao et al., 2020). Ages were taken from the  
140 “Bacon” (Blaauw and Christen, 2011) age-depth models presented in Li et al. (2022, LegacyAge 1.0),  
141 and for each record, we provide an ensemble of 1000 realizations of the age-depth model in our data  
142 product so that it can be used to account for chronological uncertainty on the reconstructions. As the  
143 chronological and reconstruction errors are independent, they can be added in quadrature to obtain the  
144 combined error. With this information, users can easily produce curves with all relevant uncertainties as  
145 exemplary shown in Appendix Figure 1.

146 We compiled the fossil data into four sub-continental datasets for Eastern North America ( $<104^{\circ}\text{W}$ ;  
147 Williams et al., 2000), Western North America, Europe ( $<43^{\circ}\text{E}$ ) and Asia ( $>43^{\circ}\text{E}$ ). We restricted the  
148 analyses to the 70 most common taxa on each continent to reduce computational power after making  
149 sure that higher taxa number would not substantially improve model statistics in climate reconstructions.  
150 The number of taxa is limited by the modern training dataset from North America, which contains 70  
151 taxa after applying our taxa harmonization routine (see details in Herzschuh et al., 2022c). We therefore  
152 restricted the number of taxa in all fossil datasets to keep the taxa comparable for the reconstructions.  
153 To identify the most common taxa we used Hill’s N2 diversity index (i.e., the effective number of  
154 occurrences of a species in the dataset; Hill, 1973). For all analyses, square-root percentages were  
155 used if not indicated otherwise.

156 A modern pollen training dataset comprised of 15379 sites includes datasets from Eurasia (EMPD1,  
157 Davis et al. 2013; EMPD2, Davis et al. 2020; Herzschuh et al., 2019; Tarasov et al., 2011) and North  
158 America (Whitmore et al., 2005). The modern pollen datasets were taxonomically harmonized in  
159 accordance with the fossil pollen dataset.

160 The site-specific  $T_{\text{ann}}$ ,  $T_{\text{July}}$ ,  $P_{\text{ann}}$  were derived from WorldClim 2 version 2.1 (spatial resolution of 30  
161 seconds ( $\sim 1 \text{ km}^2$ ), <https://www.worldclim.org>; Fick and Hijmans, 2017) by extracting the climate data at  
162 the location of the modern sample sites using the *raster* package in R (version 3.5-11, Hijmans et al.,  
163 2021; R Core Team, 2020). The WorldClim 2 dataset provides spatially interpolated gridded climate  
164 data aggregated from weather stations as temporal averages between 1970-2000 (Fick and Hijmans,

165 2017). We used monthly average temperature data to extract the mean  $T_{\text{July}}$  and the “bioclimatic  
166 variables” bio1 ( $T_{\text{ann}}$ ) and bio12 ( $P_{\text{ann}}$ ).

167

## 168 2.2 Reconstruction methods

169 Our reconstruction approach included MAT (Overpeck et al., 1985) and WA-PLS (ter Braak and Juggins,  
170 1993) by applying the MAT and WAPLS functions from the *rioja* package (version 0.9-21, Juggins, 2019)  
171 for R (R Core Team, 2020) on our Northern Hemispheric fossil pollen synthesis. For each fossil location,  
172 we calculated the geographic distance between each modern sampling site and the fossil pollen record  
173 using the *rdist.earth* function from the *fields* R-package (version 10.3, Nychka et al., 2020) and selected  
174 a unique calibration set from modern sites within a 2000 km radius. We fixed the radius to 2000 km  
175 instead of 1500 km as suggested from a study in Eastern Asia by Cao et al. (2017), because the modern  
176 dataset density is rather low in Northern Asia. For the reconstruction with MAT, we used the original  
177 pollen percentages of the selected fossil pollen taxa, looking for 7 analogues between the pollen data  
178 and the selected calibration dataset. The dissimilarity between the fossil samples and the modern pollen  
179 assemblages was determined by squared-chord distance of the percentage data (Simpson, 2012; Cao  
180 et al., 2014).

181 In addition to the classic WA-PLS reconstruction, we also propose WA-PLS\_tailored. This approach  
182 addresses the problem that co-variation of climate variables today in space is transferred to the  
183 reconstruction even if the past temporal relationship among the climate variables mechanistically differs.  
184 In fact, this approach aims to make use of the full climate space covered by the modern pollen samples  
185 avoiding those samples in the calibration set that cause spatial covariation. This approach is based on  
186 the assumption that several climate variables can be reflected in one and the same pollen assemblage  
187 because different plant taxa have different optima in temperature and precipitation ranges and might  
188 therefore occur with different co-occurrence and abundance pattern. To reconstruct  $T_{\text{July}}$  we identified  
189 the  $P_{\text{ann}}$  range reconstructed by WA-PLS and extended it by 25% to both ends of the modern  $P_{\text{ann}}$  range  
190 in order to reduce the influence of  $P_{\text{ann}}$  on  $T_{\text{ann}}$  and  $T_{\text{July}}$  reconstruction due to co-variation. We applied  
191 the same method to the reconstruction of  $P_{\text{ann}}$ .  $T_{\text{ann}}$  and  $T_{\text{July}}$  were tailored by  $P_{\text{ann}}$ ;  $P_{\text{ann}}$  was tailored by  
192  $T_{\text{July}}$  and, additionally, by  $T_{\text{ann}}$  (illustrated for an example in Appendix Fig. 2). Reconstruction  
193 uncertainties are provided as root mean square errors (RMSE) derived from the output in the MAT and

194 WAPLS functions. Model errors of WA-PLS and MAT are reported as root mean square error of  
195 prediction (RMSEP) derived from leave-one-out cross-validation.

196 We provide site- or sample-specific measures of quality in addition to the error estimates and model  
197 statistics to allow the user to assess the quality of the climate reconstruction dataset. First, we applied  
198 a Canonical Correlation Analysis (CCA) to the modern training dataset in order to explore the modern  
199 relationship between the pollen spectra and the climate variables and to infer the explained variance in  
200 the modern pollen dataset by the target climate variables (ter Braak, 1988) by using the *cca* function in  
201 the *vegan* R-package (version 2.5-7, Oksanen et al., 2020). The ratio between constrained ( $\lambda_1$ ) and  
202 unconstrained ( $\lambda_2$ ) explained variance was determined for all modern training datasets used for climate  
203 reconstructions. High values of  $\lambda_1$  vs  $\lambda_2$  ( $\geq 1$ ) are commonly considered as an indicator to measure  
204 how well the target environmental variable is related to the variation in the modern pollen data set (e.g.  
205 Juggins, 2013). However, most training data sets encompass multiple environmental variables that are  
206 often correlated and additional requirements to such variables would be necessary to explain a  
207 significant and independent portion of the variation in the training data set. While a careful design of the  
208 training data set can help reduce the effect of correlated environmental gradients, it can never eliminate  
209 them completely (Juggins, 2013). To infer the analogue quality as an indicator of no-analogue situations  
210 we calculated the minimum dissimilarity (squared chord distance) between modern pollen assemblages  
211 and fossil pollen assemblages with probability thresholds of 1% (indicating very good analogs), 2.5%  
212 (good analogs) and 5% (poor analogs) using the *minDC* function from the *analogue* R-package (version  
213 0.17-6, Simpson et al., 2021).

214 A statistical significance test (Telford and Birks, 2011) was applied using the *randomTF* function in the  
215 *palaeoSig* R-package (version 2.0-3, Telford, 2019). In this test, the proportion of variance in the fossil  
216 pollen data explained by the reconstructed environmental variable is estimated from redundancy  
217 analysis (RDA) and tested against a null distribution generated by replacing the modern training dataset  
218 with randomly generated surrogate fields. The surrogate fields were simulated to have realistic spatial  
219 autocorrelation by fitting variograms to the WorldClim 2 temperature and precipitation data; 1000-  
220 member ensembles were simulated for each variable. A reconstruction is considered statistically  
221 significant if the reconstructed variable explains more of the variance than 95% of the random  
222 reconstructions (Telford and Birks, 2011). The reconstructed climate variables were tested as



223 introducing the environmental variable as a single variable in a run, as well as with partialling out the  
224 explained variance in the pollen data by the respective other variables.

225 We used Plantaginaceae (mostly representing *Plantago lanceolata*-type in Europe) and *Rumex*-type to  
226 assess human influence as an indicator for intense herding (Behre, 1988). In addition, we calculated the  
227 correlation between the WA-PLS reconstruction of  $T_{\text{July}}$ ,  $T_{\text{ann}}$  and  $P_{\text{ann}}$  and the pollen percentages of  
228 Plantaginaceae and *Rumex* for 9000, 3000 and 1000 years BP to assess potential biases in the dataset.

229

### 230 **3 Dataset description LegacyClimate 1.0: input data, reconstructions and reconstruction model** 231 **statistics**

232 LegacyClimate 1.0 provides pollen-based reconstructions and sample-specific reconstruction errors of  
233  $T_{\text{ann}}$ ,  $T_{\text{July}}$  and  $P_{\text{ann}}$  for 2594 fossil pollen records (i.e., a total of 146067 single pollen samples) from three  
234 reconstruction methods (WA-PLS, WA-PLS\_tailored, MAT). Furthermore, we provide the method-  
235 specific model metadata and quality measures for each record and each climate variable (Table 1). To  
236 ease data handling, the dataset files are separated into Western North America, Eastern North America,  
237 Europe and Asia.

238

239

240

241

242

243

244

245

246

247

248

249 **Table 1.** Structure and content of the LegacyClimate 1.0 data with details about the information  
 250 contained in the input datasets, in the climate reconstructions and the reconstruction model statistics.

Datasets	Content
<b>Input datasets</b>	Modern pollen dataset of 15379 sites
	Modern dataset of $T_{ann}$ , $T_{July}$ , $P_{ann}$
	Fossil pollen data (LegacyPollen 1.0) for 2594 sites with a total of 146067 samples
	Bacon age-depth models (LegacyAge 1.0) for 2579 sites
<b>LegacyClimate 1.0: Climate reconstructions</b>	Reconstructions and sample-specific reconstruction errors of $T_{ann}$ , $T_{July}$ and $P_{ann}$ for 2593 sites using MAT, WA-PLS and WA-PLS_tailored
	Ensemble of 1000 realizations of the Bacon age-depth models for 2579 sites
<b>LegacyClimate 1.0: Reconstruction model statistics</b>	<b>Site information</b> (Event label, Source, ID, Site name, Longitude, Latitude)
	<b>Modern pollen dataset information</b> (number of modern analogues, range of climate variables)

**Model statistics for each site for MAT, WA-PLS, WA-PLS\_tailored** (including  $r^2$  observed vs. predicted, RMSEP, no. of WA-PLS components)

---

**LegacyClimate 1.0: Quality Measures**

**Canonical Correlation Analysis (CCA)** of the modern training dataset

**Minimum dissimilarities** between modern pollen assemblages and fossil pollen assemblages for each record sample for MAT

**Statistical significances** sensu Telford & Birks (2011) for each site for MAT, WA-PLS, WA-PLS\_tailored

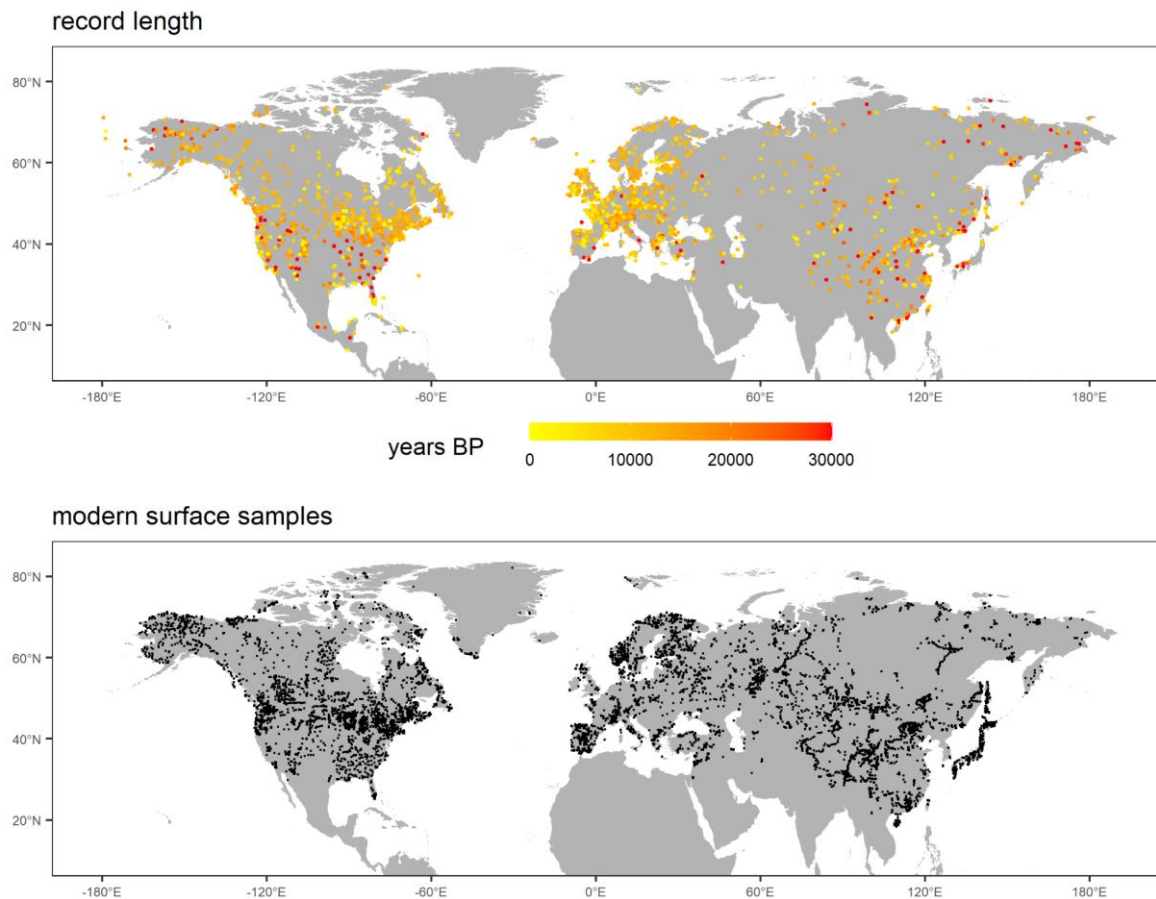
---

251

252 **4 Dataset assessment**253 **4.1 Spatial and temporal coverage of LegacyClimate 1.0**

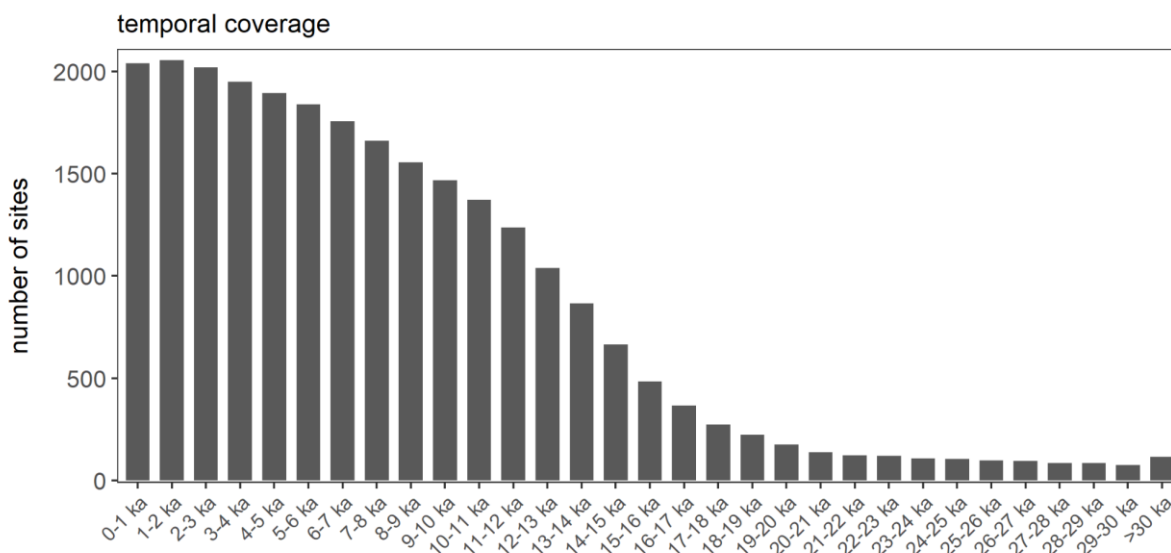
254 In total, we provide reconstructions for 2594 fossil pollen records. Among them 670 records are located  
 255 in Eastern North America, 361 records in Western North America, 1075 records in Europe and 488  
 256 Asian records (Fig. 1). Some few records are included that come from marine cores which were taken  
 257 from the continental shelf. They contain information from source areas from the nearby continents (e.g.  
 258 fluvially transported material). If users want to focus on terrestrial-only records, those marine sites could  
 259 be filtered out by the archive type provided in the metadata. Climate reconstructions for one fossil record  
 260 in the Western North American Dataset on Hawaii (Dataset-ID 17832, "Kealia Pond") could not be  
 261 performed as there were no modern training data available within a 2000 km area.

262 The temporal coverage of the records is rather uneven: 75 and 666 records cover the periods between  
 263 30-29 ka and 15-14 ka, respectively (Fig. 2).



264

265 **Figure 1.** Upper panel: map indicating the spatial distribution and record lengths covered by the  
266 LegacyPollen 1.0 dataset (Herzschuh et al., 2022c) for which climate reconstructions, temporal and  
267 reconstruction uncertainties and reconstruction quality measures are provided in LegacyClimate 1.0 with  
268 a total of 2594 records; Lower panel: spatial distribution of modern pollen dataset used for reconstruction  
269 with a total of 15379 sites.



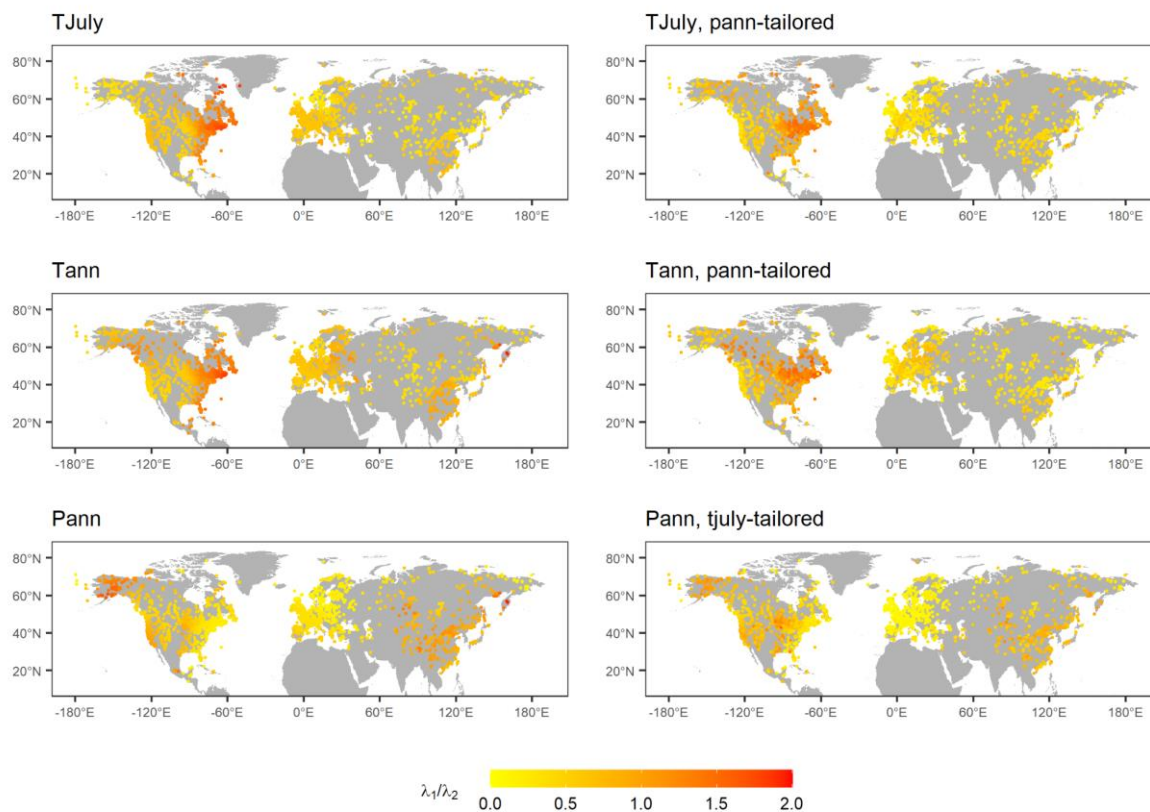
270

271 **Figure 2.** Number of records that cover certain millennia of the last 30 ka.

272

#### 273 **4.2 Modern relationships between pollen and climate assessed by constrained ordination.**

274 Results from CCA applied to modern datasets reveal that  $T_{\text{July}}$ -constrained ordinations have high  $\lambda_1/\lambda_2$   
 275 ratios, indicating a strong relationship between this climate variable and modern pollen assemblages, in  
 276 Eastern North America while low ratios can be found in Central Asia. The spatial pattern of  $\lambda_1/\lambda_2$  of  
 277 ordinations constrained by  $T_{\text{ann}}$  is overall similar to those of  $T_{\text{July}}$  but the ratios are slightly higher for  $T_{\text{ann}}$   
 278 than for  $T_{\text{July}}$ . Reconstructions for  $P_{\text{ann}}$  show low ratios in Europe and Eastern North America. Areas with  
 279 high ratios are concentrated in Alaska and East Asia (Fig. 3).



280

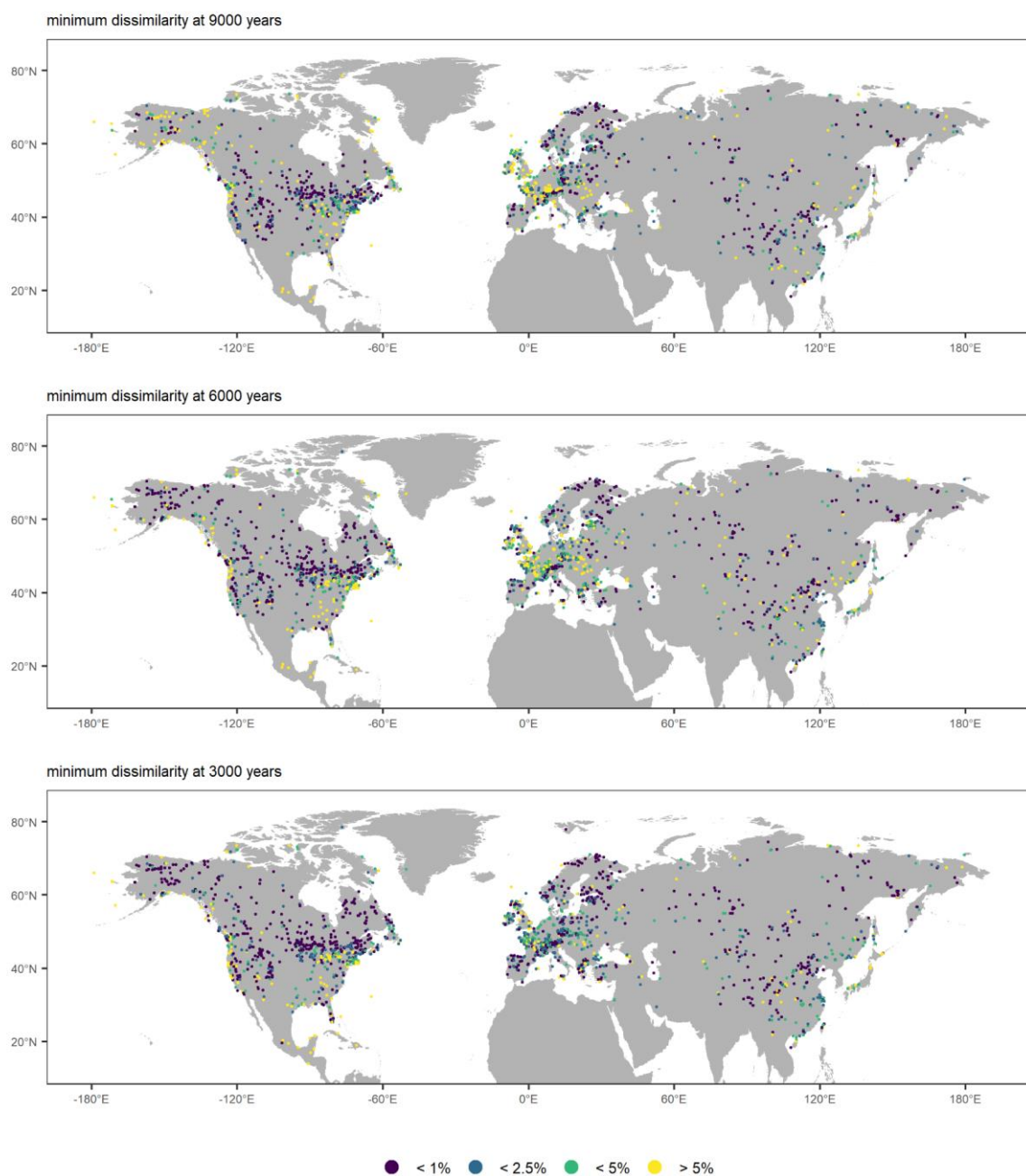
281 **Figure 3.** Maps showing  $\lambda_1/\lambda_2$ , representing the ratio of explained variance of first axis (constrained) vs.  
 282 second (unconstrained) axis as revealed by applying a CCA to all modern training datasets that were  
 283 used for the reconstructions. High ratios ( $\geq 1$ ) indicate a strong relationship between the modern pollen  
 284 datasets and climate and can be used to determine ecologically important determinants. Constraining  
 285 variables as well as tailoring of the dataset (see methods) is indicated in the map captions.

286

### 287 4.3 Analogue quality

288 The dissimilarity (squared chord distance) between modern pollen assemblages and fossil pollen  
 289 assemblages was calculated and extracted for distinct time-slices at 9000, 6000 and 3000 years BP. In  
 290 total, 36.4% (9000 years BP), 39.2% (6000 years BP) and 45.6% (3000 years BP) records indicate a  
 291 very good (<1%) analogue quality. The central part of the North American continent, Scandinavia and  
 292 Central Asia show a very good analogue quality for all time-slices investigated. Poor (<5%) analogues  
 293 can be found in Western Europe, the eastern parts of the United States and along the eastern Asian  
 294 coastline. Non-analogues (>5%) are found for 22.6% (9000 years BP), 20.47% (6000 years BP) and  
 295 12.5% (3000 years BP) record respectively, especially in Western Europe and at 9000 years BP in  
 296 Alaska (Fig. 4).

297



298

299 **Figure 4.** Analogue quality as assessed by squared chord distance between modern pollen  
 300 assemblages and fossil pollen assemblages. Results identify very good (<1%), good (<2.5%) and poor  
 301 (<5%) analogues. Distances >5% are considered to indicate non-analogue situations (as percentage of  
 302 all distances among pollen samples in the modern dataset used for calibration).

303

304

305

#### 306 4.4 Prediction errors of LegacyClimate 1.0

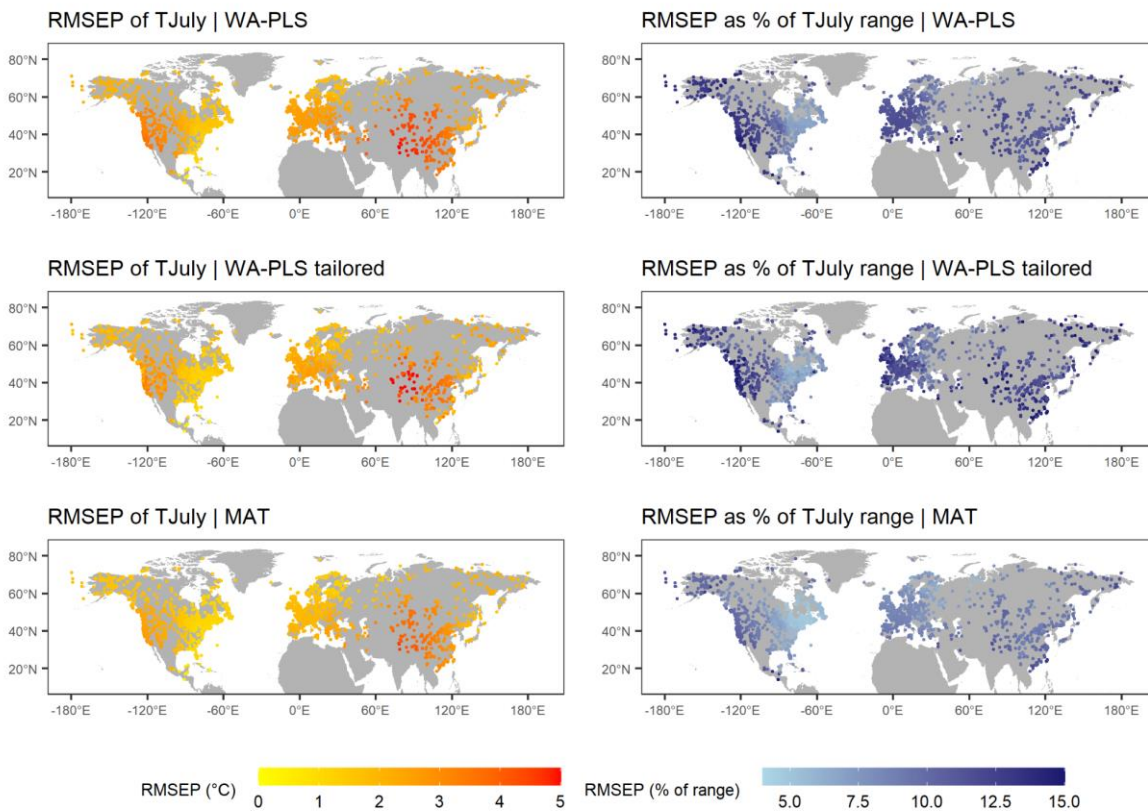
307 The mean RMSEPs and their standard deviations for  $T_{\text{ann}}$  are  $1.98 \pm 0.52^\circ\text{C}$  (MAT),  $2.61 \pm 0.53^\circ\text{C}$  (WA-  
308 PLS) and  $2.24 \pm 0.61^\circ\text{C}$  (WA-PLS\_tailored) and mean RMSEPs as a percentage of modern  $T_{\text{ann}}$  range  
309 are  $7.68 \pm 1.93\%$  (MAT),  $10.09 \pm 2.05\%$  (WA-PLS) and  $10.26 \pm 2.79\%$  (WA-PLS\_tailored). The largest  
310 mean RMSEP values are located in Central Asia in Kazakhstan, Mongolia and the north-western parts  
311 of the Tibetan Plateau and are consistent across all three reconstruction methods. Other areas with  
312 large mean RMSEP values are located in Western North America, Southern and Central Europe and  
313 south-east Asia. The smallest RMSEPs can be found along the east coast of North America. Relative  
314 to the modern temperature range, the RMSEP from this region also reveals the lowest fraction. In  
315 general, MAT has the lowest mean error fraction relative to the modern temperature range of all three  
316 methods.

317 The mean RMSEPs of  $T_{\text{July}}$  are  $1.90 \pm 0.63^\circ\text{C}$  (MAT),  $2.50 \pm 0.73^\circ\text{C}$  (WA-PLS) and  $2.21 \pm 0.75^\circ\text{C}$  (WA-  
318 PLS\_tailored) and mean percentages of  $T_{\text{July}}$  range are  $8.11 \pm 1.64\%$  (MAT),  $10.71 \pm 1.94\%$  (WA-PLS)  
319 and  $10.70 \pm 2.60\%$  (WA-PLS\_tailored). Thus, they are slightly smaller than those of  $T_{\text{ann}}$  but slightly larger  
320 as a percentage of the range. The spatial patterns, however, are largely similar to those of  $T_{\text{ann}}$ .

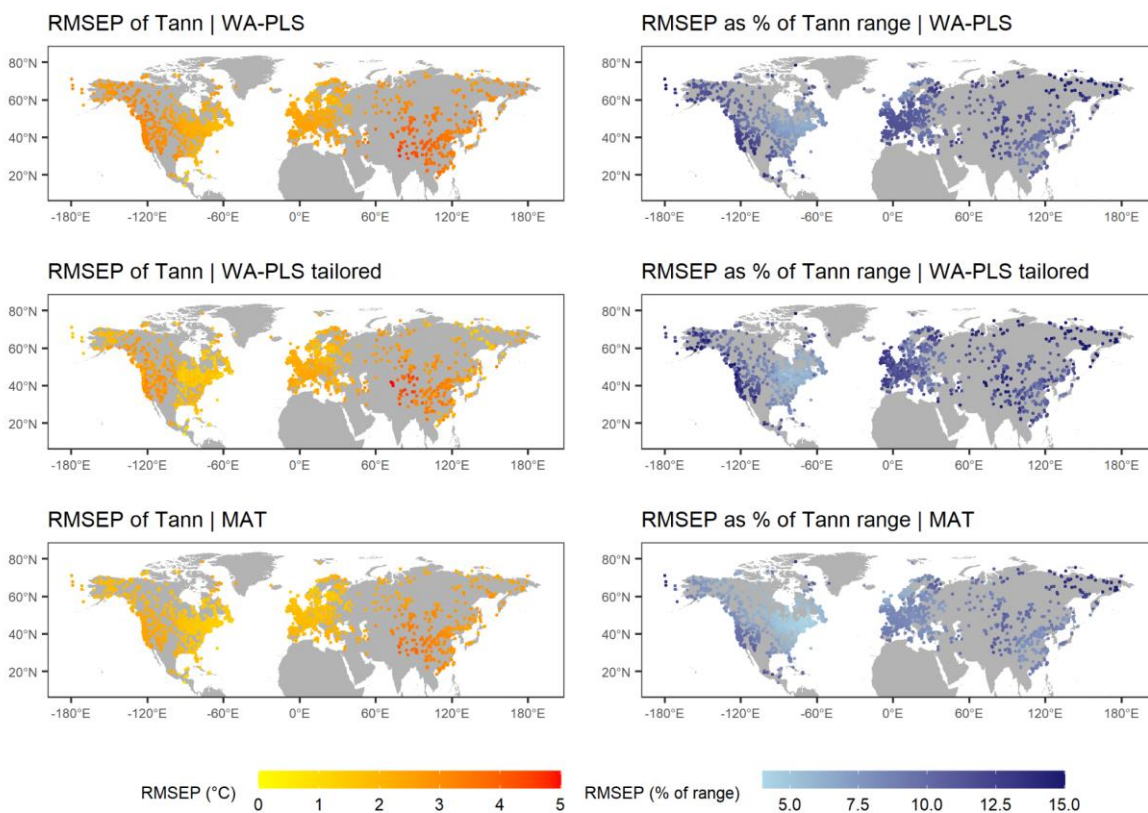
321 The mean RMSEPs of  $P_{\text{ann}}$  are  $176.38 \pm 51.40$  mm (MAT),  $244.48 \pm 75.84$  mm (WA-PLS) and  
322  $232.71 \pm 98.57$  mm (WA-PLS\_tailored) and mean percentages of  $P_{\text{ann}}$  range are  $6.78 \pm 1.48\%$  (MAT),  
323  $9.27 \pm 1.70\%$  (WA-PLS) and  $10.26 \pm 2.67\%$  (WA-PLS\_tailored). High RMSEPs are found for Western  
324 North America, Europe and along the coastline of south-east Asia, while the lowest RMSEP values are  
325 found for Central Asia. A clear division in RMSEPs are found on the North American continent: while  
326 the western part of North America (with the exception of Alaska) has a rather high RMSEP, the eastern  
327 part of North America has a smaller RMSEP. This pattern is found for all three methods (Fig. 5).

328

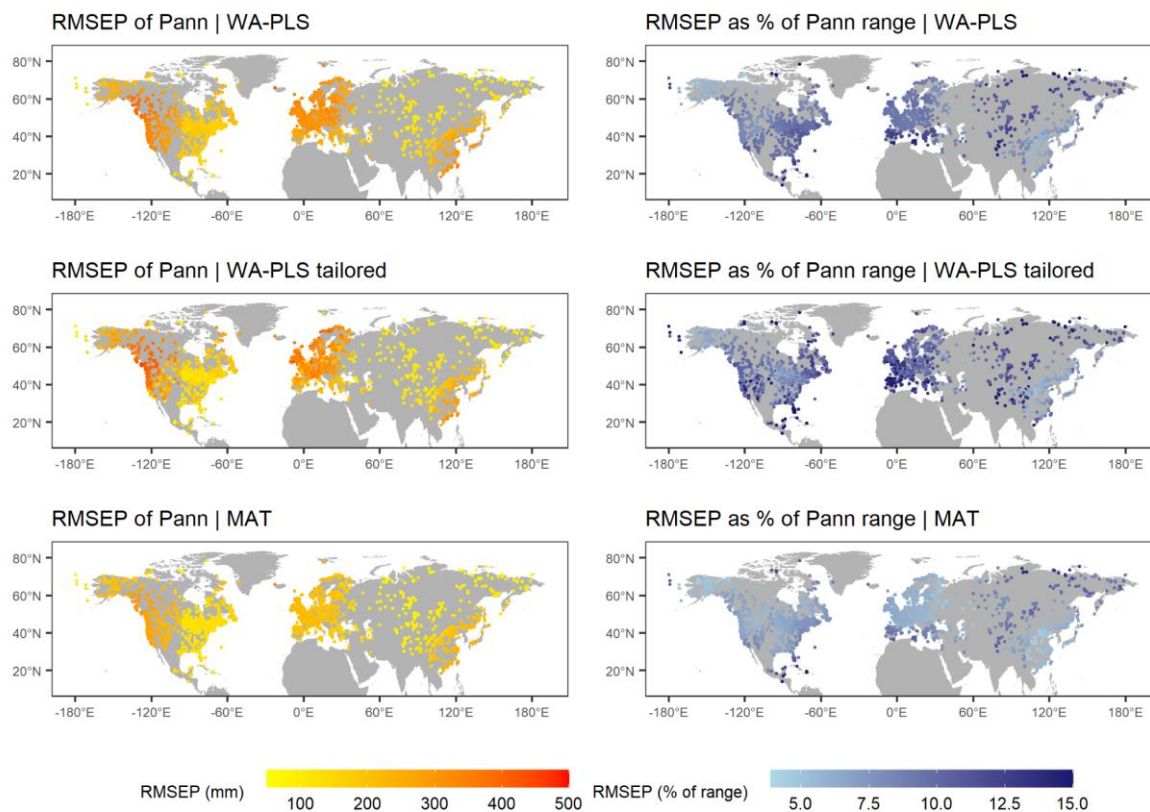




329



330



331

332 **Figure 5.** Spatial distribution of root-mean-squared error of prediction (RMSEP) as inferred from leave-  
 333 one-out cross-validation presented as absolute values and as a percentage of the range of mean July  
 334 temperature ( $T_{\text{July}}$ ), mean annual temperature ( $T_{\text{ann}}$ ), annual precipitation ( $P_{\text{ann}}$ ) in the modern pollen  
 335 data used for reconstruction for the three methods applied (Weighted-Averaging Partial-Least Squares  
 336 regression (WA-PLS), WA-PLS using a training set from within a limited climate range (WA-  
 337 PLS\_tailored) and Modern Analogue Technique (MAT)).

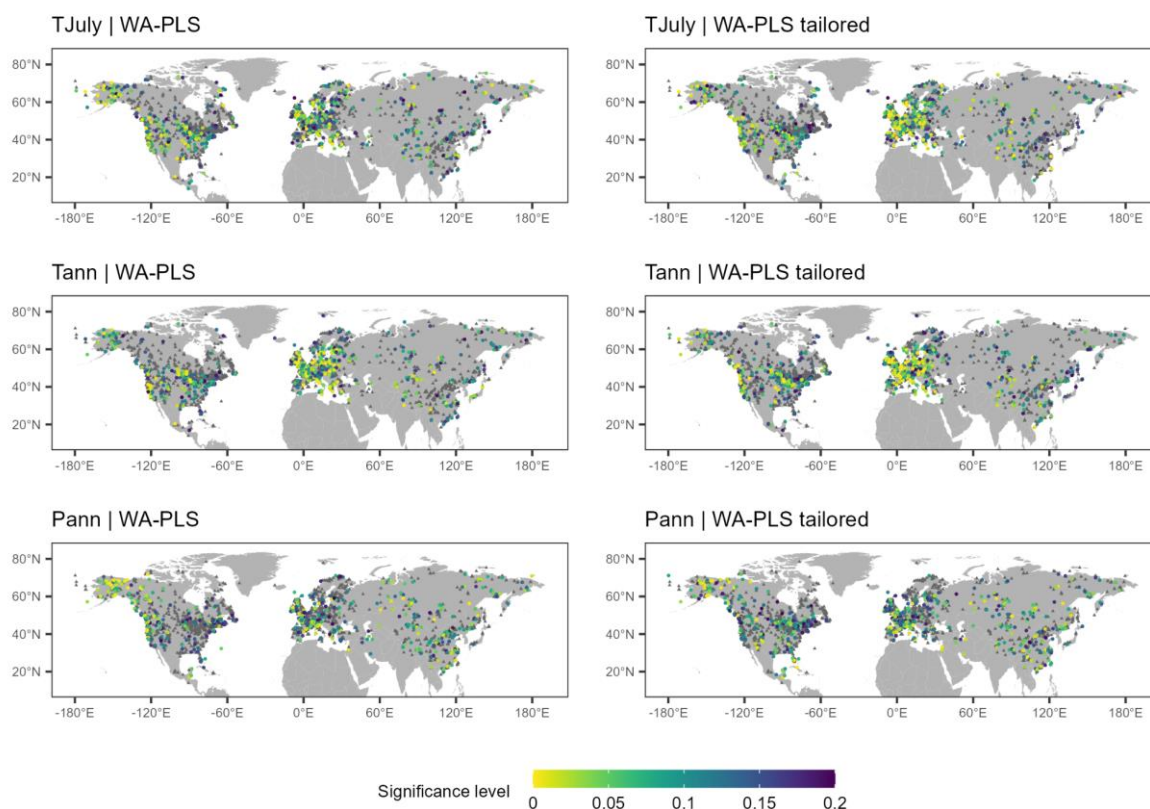
338

#### 339 4.5 Significance test

340 A significance test ( $p < 0.1$  and in addition  $p < 0.2$ , see methods) according to Telford and Birks (2011)  
 341 was performed for each record (Fig. 6; Table 2). For the  $T_{\text{July}}$  reconstruction, 16.4% [ $p < 0.2$ : 27.2%] (WA-  
 342 PLS) and 19.0% [ $p < 0.2$ : 29.1%] (WA-PLS\_tailored) of all records passed the significance test when  
 343 included as a single variable in the significance test. Partialling out precipitation as a conditional variable  
 344 causes an increase in the amount of significant records to 19.0% [ $p < 0.2$ : 30.6%] for WA-PLS of  $T_{\text{July}}$ ,  
 345 but a decrease for WA-PLS\_tailored to 16.7% [ $p < 0.2$ : 27.6%] of all records. The  $T_{\text{ann}}$  reconstruction is  
 346 significant for 16.5% [ $p < 0.2$ : 27.1%] (WA-PLS) and 20.0% [ $p < 0.2$ : 31.6%] (WA-PLS\_tailored) of all  
 347 records when tested as a single variable. When partialling out precipitation, the amount of significant

348 records slightly increases for WA-PLS, but decreases for WA-PLS\_tailored. 13.0% [ $p < 0.2$ : 21.8%] (WA-  
 349 PLS) and 14.3% [ $p < 0.2$ : 25.4%] (WA-PLS\_tailored) of all records pass the significance test when testing  
 350  $P_{ann}$  as a single variable. Partialling out the mean July temperature as a conditional variable increases  
 351 the number of significant records for both WA-PLS and WA-PLS\_tailored.

352



353

354 **Figure 6.** Maps showing mean July temperature ( $T_{July}$ ), mean annual temperature ( $T_{ann}$ ), annual  
 355 precipitation ( $P_{ann}$ ) records that passed the reconstruction significance test ( $p < 0.2$ ). Colors indicate the  
 356 significance level. Records that did not pass the significance level ( $p \geq 0.2$ ) are shown as grey  
 357 rectangles.

358

359

360

361

362 **Table 2.** Percentage of records that pass the reconstruction significance test ( $p < 0.1$  and  $p < 0.2$ ) sensu  
 363 Telford and Birks (2011). The values in brackets for  $p < 0.1$  indicate the significance values without taking  
 364 spatial autocorrelation into account.

	WA-PLS		WA-PLS_tailored		MAT	
	$p < 0.1$	$p < 0.2$	$p < 0.1$	$p < 0.2$	$p < 0.1$	$p < 0.2$
$T_{July}$	16.4%	27.2%	19.0%	29.1%	44.1%	56.8%
	(30.9%)		(35.2%)		(42.4%)	
$T_{July}$ partialling out $P_{ann}$	19.0%	30.6%	16.7%	27.6%	48.7%	61.4%
	(35.5%)		(33.6%)		(39.9%)	
$T_{ann}$	16.5%	27.1%	20.0%	31.6%	46.5%	57.7%
	(32.8%)		(36.1%)		(42.4%)	
$T_{ann}$ partialling out $P_{ann}$	16.7%	27.1%	18.4%	28.8%	48.1%	61.9%
	(32.6%)		(34.1%)		(39.2%)	
$P_{ann}$	13.0%	21.8%	14.3%	25.4%	36.5%	51.1%
	(32.1%)		(33.4%)		(36.3%)	
$P_{ann}$ partialling out $T_{July}$	14.5%	24.1%	16.5%	28.2%	39.4%	53.7%
	(34.2%)		(36.5%)		(34.5%)	

365

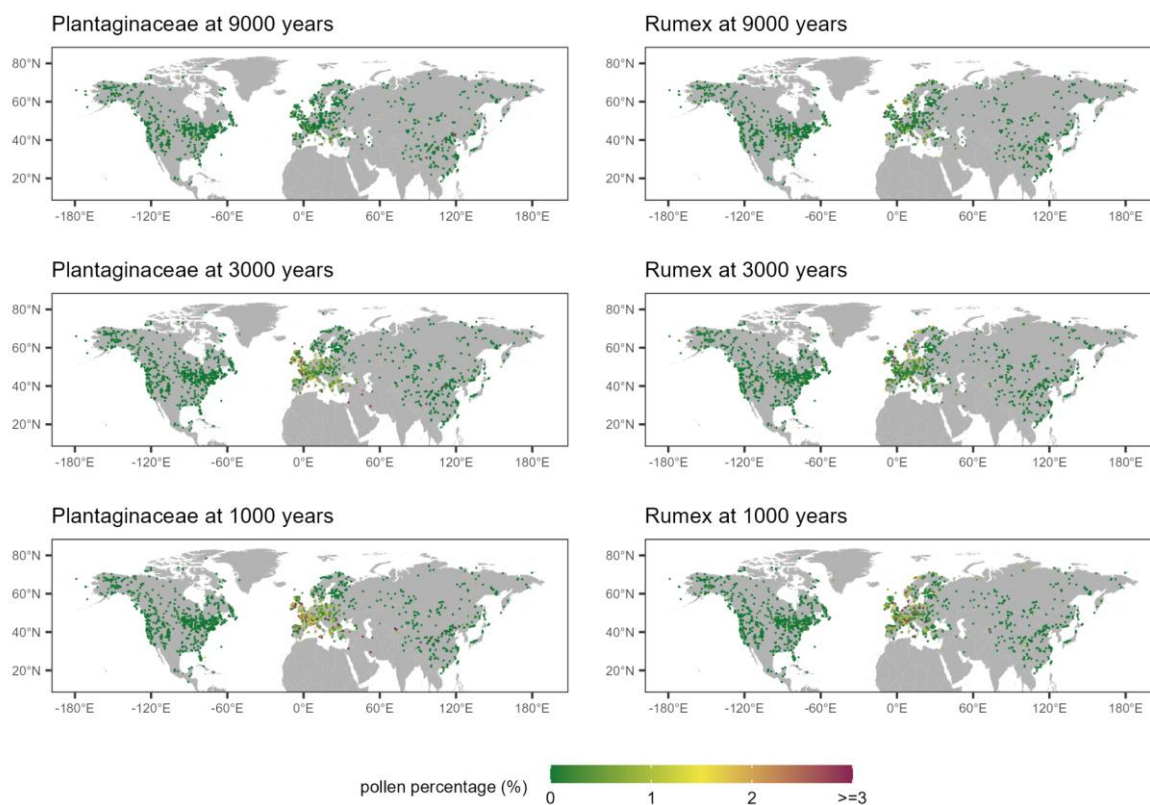
366

367

368 **4.6 Human impact**

369 We used the abundance of Plantaginaceae and *Rumex* as indicators of grazing and such intense animal  
 370 husbandry. Overall weak human impact is inferred for North America and Northern Asia. The indicators  
 371 show strong human impact only in individual records at 9000 years BP in China and the Mediterranean  
 372 region (Fig. 7). The percentage values of Plantaginaceae and *Rumex* were high especially in Europe  
 373 for 3000 years and 1000 years BP which indicates growing human impact on that region. High  
 374 Plantaginaceae correlate with low  $T_{\text{July}}$  and high  $P_{\text{ann}}$  in Central Europe indicating potential biases in the  
 375 temperature reconstructions i.e. too low temperatures become reconstructed. Similar correlations are  
 376 found for *Rumex*, especially in Northern Europe (Fig. 8).

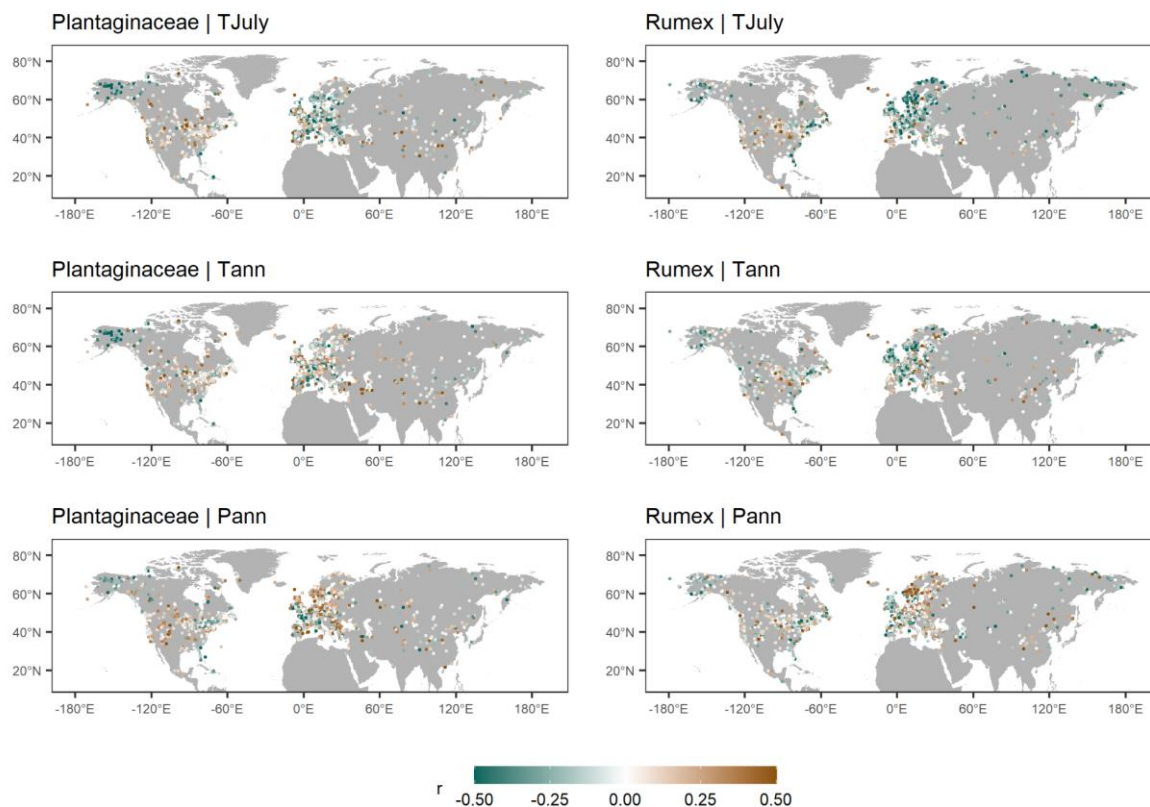
377



378

379 **Figure 7.** Abundance of Plantaginaceae (left) and *Rumex* (right) at 9000, 3000 and 1000 years BP.

380 Colors indicate percentage values.



381  
 382 **Figure 8.** Correlation between the percentage of Plantaginaceae (left) and *Rumex* (right) and  
 383 reconstructed  $T_{July}$ ,  $T_{ann}$  and  $P_{ann}$  with WA-PLS.

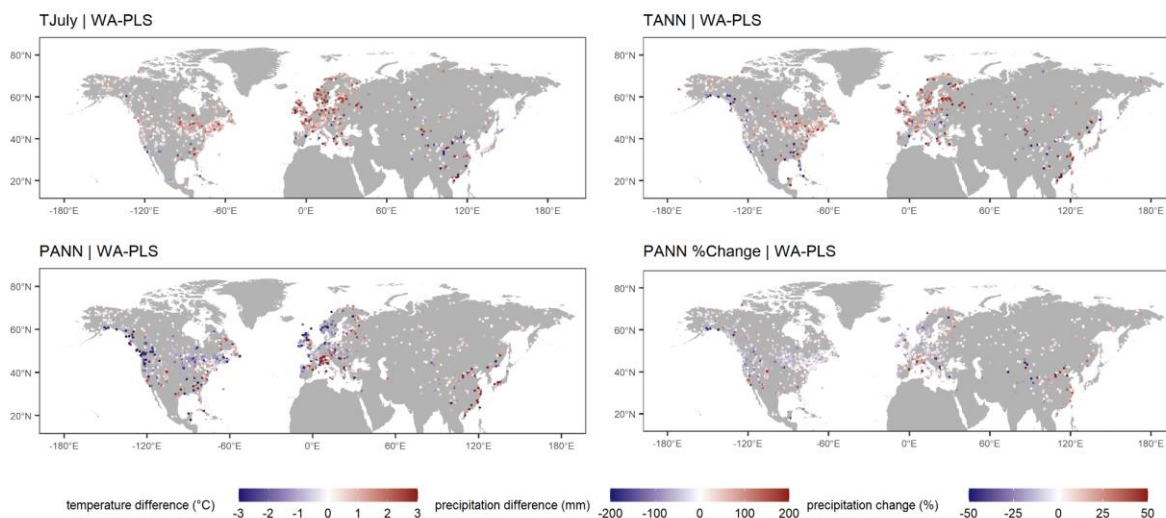
384

#### 385 4.7 Assessment of major temporal patterns of LegacyClimate 1.0

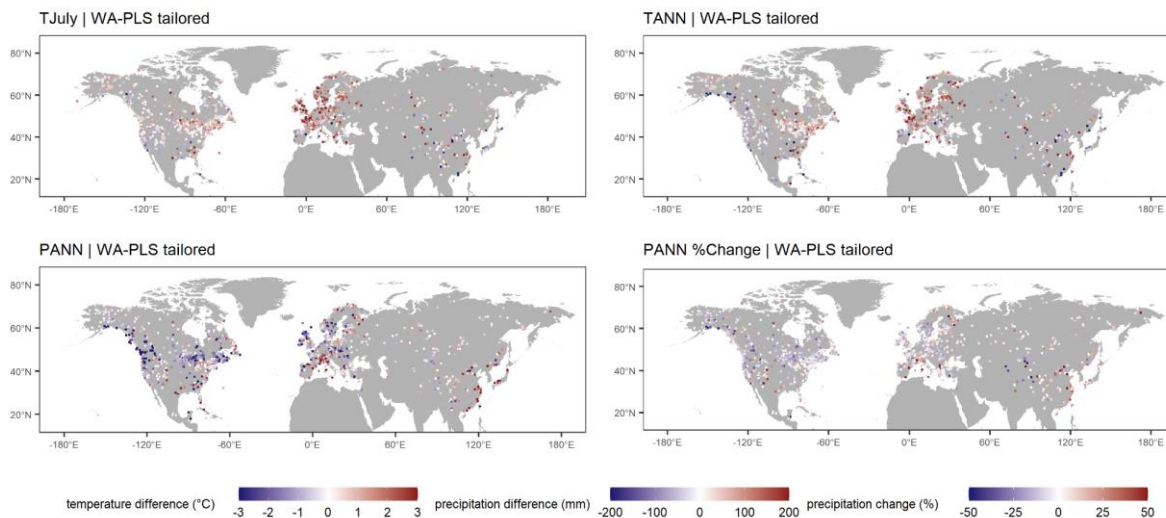
386 To illustrate the difference between Mid- and Late Holocene climate, we calculated the value for the  
 387 three climate variables at 6 ka BP and 1 ka BP, each time taking the average of the interpolated values  
 388 at those ages for the ensemble of 1000 realizations of the age-depth models (Li et al., 2022). Differences  
 389 between these time-slices reveal warmer and drier conditions during the Mid-Holocene compared with  
 390 Late Holocene conditions, especially in Eastern North America, but also in Central and Northern Europe.  
 391 The overall patterns are in good agreement for all three methods but show differences on a regional  
 392 scale, especially when comparing the reconstructions with WA-PLS and MAT. For  $T_{July}$ , the  
 393 reconstruction with MAT shows greater temperature differences in Western North America and south-  
 394 east Asia. Compared to the reconstruction with WA-PLS, there is a reduced cooling from 6 ka to 1 ka in  
 395 Eastern Europe and a warming instead of a cooling in the Western Mediterranean region and along the  
 396 south-eastern Asian coastline in MAT. For large areas in North America and Europe, the reconstructions  
 397 with WA-PLS suggest an increase in precipitation from 6 to 1 ka BP. A shift to drier conditions can be

398 found along the south-eastern coastline in North America, in the Mediterranean Region and especially  
399 in south-east Asia. The reconstruction with MAT reveals a gradient from increasing precipitation in  
400 south-western Europe to decreasing precipitation in north-eastern Europe. In contrast to the  
401 reconstructions with WA-PLS, records along the south-eastern Asian coastline suggest an increase in  
402 precipitation with MAT rather than a decrease (Fig. 9).

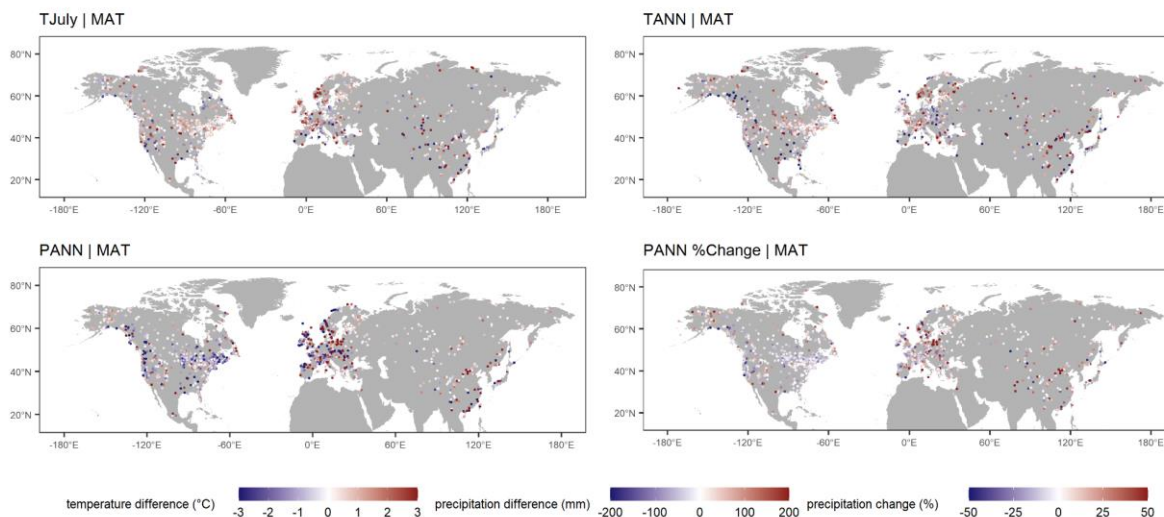
403



404

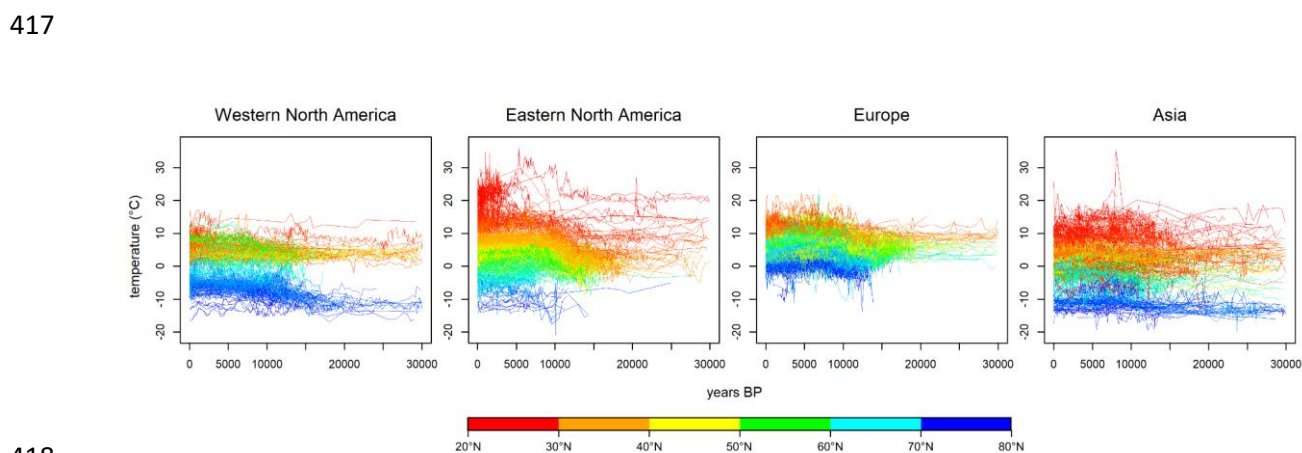


405



406  
 407 **Figure 9.** Difference from 6 ka to 1 ka for mean July temperature ( $T_{July}$ ), mean annual temperature ( $T_{ann}$ ),  
 408 annual precipitation ( $P_{ann}$ ) and  $P_{ann}\%$  as reconstructed from WA-PLS (upper panel), WA-PLS\_tailored  
 409 (middle panel) and MAT (lower panel).

410  
 411 Time-series of absolute  $T_{ann}$  reconstructions reveal temporal as well as latitudinal spatial variation on  
 412 the single continents. Eastern North America and Asia show the most variation in the low latitudes. It is  
 413 also Eastern North America which shows the most pronounced latitudinal gradient. In Western North  
 414 America, the most variation takes place in the high latitudes, while the variation is concentrated to the  
 415 mid-latitudes in Europe. Especially in North America, the warming since the last deglaciation and the  
 416 beginning of the Holocene is well shown in the temporal variation of the time-series (Fig. 10).



418  
 419 **Figure 10.** Time-series of absolute mean annual temperature ( $T_{ann}$ ) reconstruction with WA-PLS for  
 420 each (sub-)continent. Colors denote the latitude of record origin. Age and reconstruction uncertainties  
 421 are not plotted but are available for each time-series.



422

423 **4.8 Assessment of consistency among reconstruction methods**

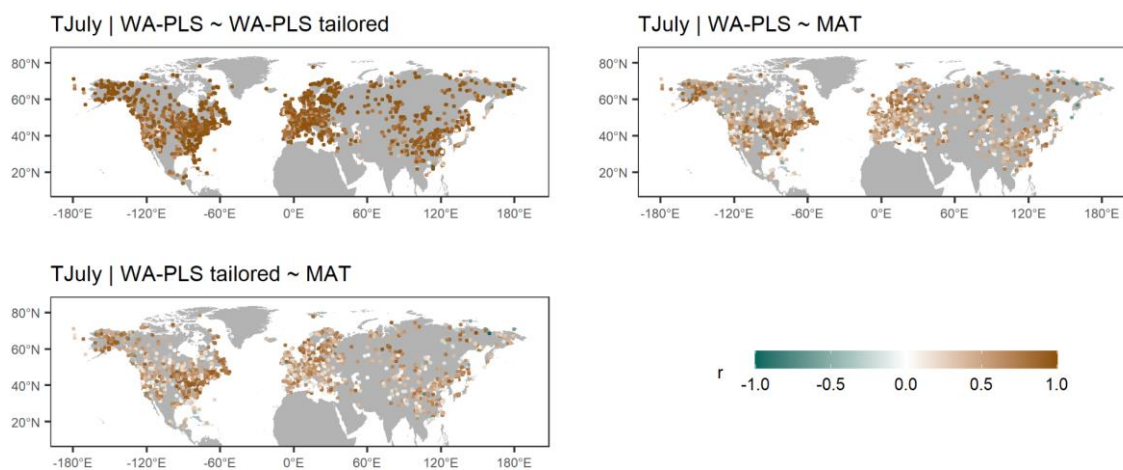
424 Reconstructions with MAT are, in general, in good agreement with those derived from the WA-PLS.

425 Comparing MAT with WA-PLS, 37.3% ( $T_{July}$ ), 38.9% ( $T_{ann}$ ) and 30.4% ( $P_{ann}$ ) of all records have a positive426 correlation of  $r \geq 0.6$ . Strong positive correlations ( $r \geq 0.9$ ) can mainly be identified in Eastern North

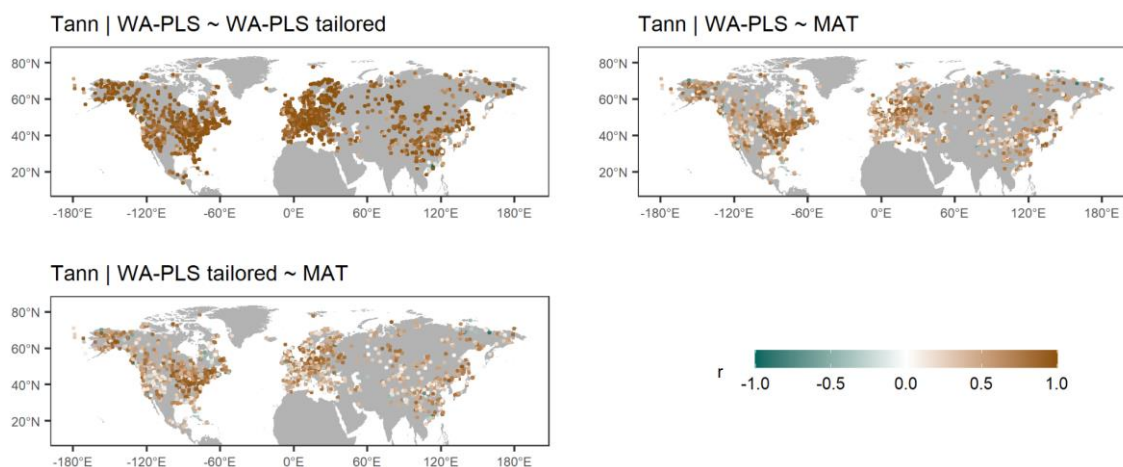
427 America, while weak correlation can be found for large areas in central North America and most of

428 Europe (Fig. 11).

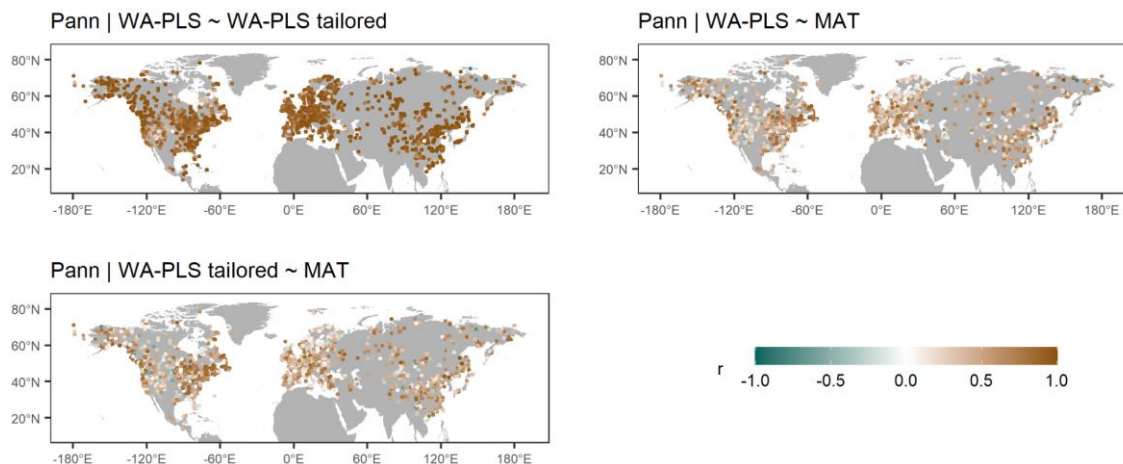
429



430



431

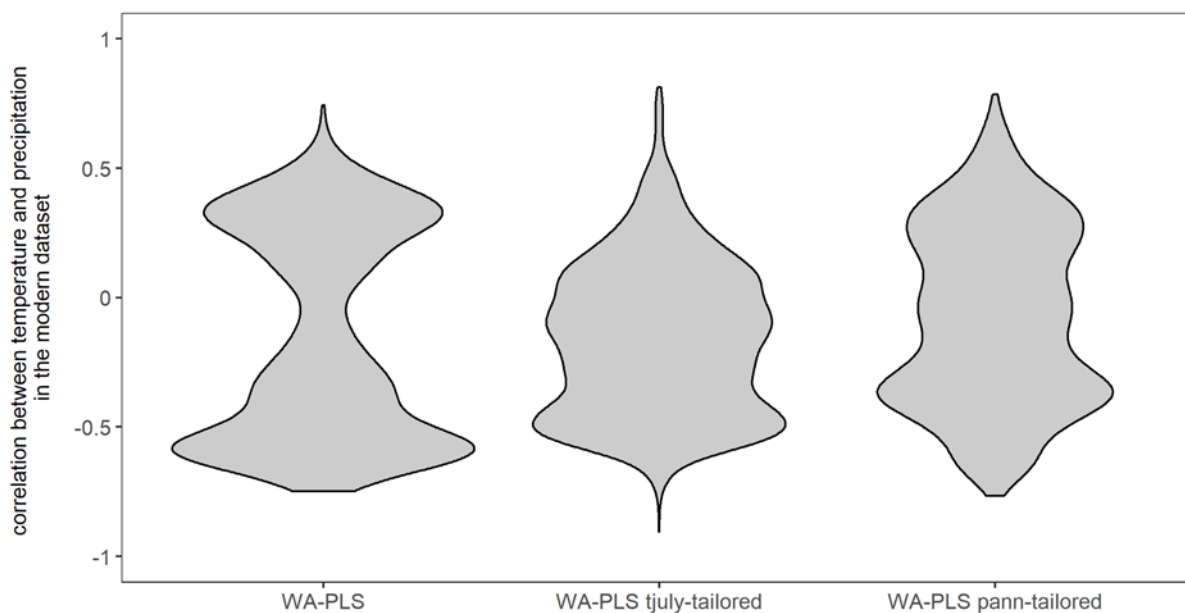


432

433 **Figure 11.** Correlation between time-series of the 3 different reconstruction methods used - weighted-  
 434 averaging partial least squares using a global training set (WA-PLS), WA-PLS using a training set with  
 435 a limited modern climate range (WA-PLS\_tailored) and the modern analogue technique (MAT) for the  
 436 three climate variables of mean July temperature ( $T_{July}$ ), mean annual temperature ( $T_{ann}$ ) and annual  
 437 precipitation ( $P_{ann}$ ).

438

439 WA-PLS\_tailored used a reduced modern training dataset (illustrated for an example in Appendix Fig.  
 440 2). The tailoring successfully reduced the co-variation of temperature and precipitation in the modern  
 441 dataset as indicated by the distribution of the correlation coefficient in Fig. 12. Nevertheless, the obtained  
 442 reconstructions are largely consistent between WA-PLS and WA-PLS-tailored: a correlation of  $r \geq 0.9$   
 443 is found for 59.2% of all records for  $T_{July}$ , 60.7% for  $T_{ann}$  and 56.5% for  $P_{ann}$ .



444

445 **Figure 12.** Violin plot of the correlation coefficients between  $T_{\text{July}}$  and  $P_{\text{ann}}$  in the 15379 training datasets  
 446 used for the reconstructions. Left: used for WA-PLS reconstructions; middle: WA-PLS  $T_{\text{July}}$ -tailored  
 447 (used for the reconstruction of  $P_{\text{ann}}$ ); WA-PLS  $P_{\text{ann}}$ -tailored (used for the reconstruction of  $T_{\text{July}}$ ).

448

## 449 5 Discussion

### 450 5.1 Impact of the fossil pollen data source on LegacyClimate 1.0 quality

451 LegacyClimate 1.0 contains reconstructions of climate variables from fossil pollen data derived from  
 452 open-access data repositories. The fossil records were derived from multiple natural archives, most  
 453 commonly, assemblages from continuous lacustrine and peat accumulations (Herzschuh et al., 2022c).  
 454 Different sizes of lakes and peat areas result in varying sizes of pollen source areas and thus the spatial  
 455 representativeness of a record. While small lakes and peatlands are considered to provide information  
 456 about the (extra-)local scale, the regional signal is better represented in pollen assemblages from large  
 457 lakes (Jackson, 1990; Sugita, 1993). However, taphonomic changes of the records originating, for  
 458 example, from lake level changes may impact the reconstructed climate. Pollen from azonal riverine  
 459 vegetation might be over-represented in fluvially impacted pollen records.

460 Our dataset is based on taxonomically harmonized modern and fossil pollen datasets using a restricted  
 461 number of taxa. Such an approach guarantees that all records are handled consistently. Although losing  
 462 taxonomic information when merging taxa together into a higher taxonomic level, it also increases the

463 possibility of matching climate analogues in the modern and the fossil datasets. However, one needs to  
464 keep in mind that species with different ecological requirements may be merged together into one genus  
465 or family, for example, *Pinus* species that are restricted to tropical or subtropical areas in China or ones  
466 that grow in boreal forests (Cao et al., 2013; Tian et al., 2017).

467 Along with the pollen assemblages, data repositories also provide chronological information for fossil  
468 records. The quality of such chronologies varies strongly with respect to dating methods, calibration and  
469 numerical algorithms for determining an age-depth relationship (Blois et al., 2011; Trachsel and Telford,  
470 2017). Having accurate and precise chronologies is thus of pivotal importance for reconstructing past  
471 climate in order to identify temporo-spatial patterns and therefore in helping to evaluate climate model  
472 outputs. The advantage of the fossil pollen dataset used for the reconstruction presented here (i.e.,  
473 LegacyPollen 1.0; Herzschuh et al., 2022c) is that it has harmonized chronologies (LegacyAge 1.0)  
474 along with information about uncertainties as well as related metadata and scripts that allow a  
475 customized re-establishment of the chronologies (Li et al., 2022). Accordingly, we were able to provide  
476 sample specific age-uncertainties along with reconstruction uncertainties.

477

## 478 **5.2 Modern pollen and climate data sources and LegacyClimate 1.0 quality**

479 We a priori selected  $T_{\text{July}}$ ,  $T_{\text{ann}}$  and  $P_{\text{ann}}$  as target variables for our reconstructions. However, we provide  
480  $\lambda_1/\lambda_2$  (i.e. explained variance of the climate variable in the modern pollen data set relative to the variance  
481 explained by the unconstrained first axis; ter Braak, 1988), a commonly used proxy for the assessment  
482 of reconstructions. The higher  $\lambda_1/\lambda_2$  in the spatial modern dataset the higher the chance that this target  
483 climate variable has also impacted vegetation over time and is thus reflected in the variation of the fossil  
484 pollen dataset. As a rule of thumb, a ratio of 1 is considered to indicate reliable reconstructions (Juggins,  
485 2013) though useful reconstructions may also be obtained from datasets with lower values. As expected,  
486 maps of RMSEPs reveal similar spatial pattern as the results of constrained ordination. Our results  
487 indicate that in particular calibration sets from Europe have low ratios and a high RMSEP for all climate  
488 variables (despite having a high number of modern samples), likely related to the human impact on the  
489 modern and fossil data. Some areas that are known for its sensitivity to precipitation e.g. Eastern Asia  
490 show low RMSEPs as expected for  $P_{\text{ann}}$  but on the other hand show a low sensitivity to  $T_{\text{ann}}$  and  $T_{\text{July}}$ .

491 For our study we used the, to our knowledge, largest modern dataset ever used in a pollen-based climate  
492 reconstruction. For fossil pollen records in areas with an insufficient coverage of modern surface pollen  
493 samples (e.g., Central Asia or Western Siberia), it might be difficult to create a calibration dataset that  
494 maps the required variety of environmental and climatic gradients and therefore find enough modern  
495 analogues for reconstructions with a classification approach such as MAT. This is indicated by the high  
496 RMSEPs as percentages of gradient length in these areas. Our routine uses the modern pollen data  
497 from within a radius of 2000 km around the site of the fossil record. The information provided in the  
498 reconstruction metadata including number of modern pollen samples and ranges of reconstructed  
499 variables, allow an assessment of the modern dataset used for reconstruction. Our assessments of the  
500 modern dataset (e.g. using CCA), the transfer function (e.g. RMSEP) and the reconstruction (e.g. the  
501 significance test) revealed also the potential biases in the pollen-based reconstruction and pointed to  
502 limitations. Further validation and assessments of the results and more comprehensive uncertainty  
503 analyses e.g. by applying forward modelling approaches (Izumi & Bartlein, 2016; Parnell et al., 2016)  
504 would be highly valuable.

505

### 506 **5.3 Reconstruction method and LegacyClimate 1.0 quality**

507 Overall, the three reconstruction approaches, MAT, WA-PLS and WA-PLS\_tailored yield rather similar  
508 results i.e. indicated by the overall high correlation between the reconstructions of the different methods  
509 (Fig. 11). Accordingly, the major trends at global or continental scales are similar, even if the actual  
510 amplitude of change may vary locally. As each method has its own strengths and weaknesses, there is  
511 not one set of reconstructions that is absolutely superior. One advantage of our multi-method  
512 reconstruction dataset is that users can identify the methods that are likely to perform best in a selected  
513 region and/or specific reconstructions. MAT is often recommended for large-scale studies, but it is highly  
514 sensitive to the quality of analogues (Chevalier et al. 2020). Low analogue situations can arise from two  
515 causes: climate conditions that differ strongly from today (e.g., the low atmospheric CO<sub>2</sub> concentration  
516 during the LGM; Jackson and Williams, 2004), or in regions with limited modern samples (e.g.,  
517 extratropical Asia). Furthermore, growing human influence on the landscape since the Middle to Late  
518 Holocene especially in densely settled regions in Europe contributed to gaps within the potential  
519 bioclimatic space of taxa and probably also led to extinction events, especially for disturbance-  
520 dependent taxa (Zanon et al., 2018). We report the analogue distance for each sample to help identify

521 such situations. From our assessments, we revealed that analogues quality is overall rather good at  
522 least for the Holocene and except for Western Europe in particularly the British Isles (Fig. 4).

523 In contrast to MAT, WA-PLS (and most regression techniques in general) model relationships between  
524 pollen and climate and are, as such, less sensitive to the low analogue situations (Birks et al., 2010).  
525 They are, however, based on some modelling assumptions, such as the unimodality of the response of  
526 the pollen taxa to climate (ter Braak and Juggins 1993). This condition is not always met at the  
527 continental scale, primarily because of the limited taxonomic resolution of pollen data that merges  
528 several plant species with distinct climate requirements as one single pollen taxon. WA-PLS\_tailored  
529 has the same limitation but it has the advantage of reducing the influence of the correlation between  
530 variables when reconstructing, for instance, temperature and precipitation. This may be particularly  
531 relevant for regions with a temperature-moisture driven circulation system such as the East Asian  
532 Summer Monsoon (EASM) that can heavily affect precipitation patterns in certain regions (Herzschuh  
533 et al., 2019). Using WA-PLS\_tailored also increases the number of records that pass a significance level  
534 of  $p < 0.1$  (Telford and Birks, 2011). Providing several reconstructions based on different assumptions  
535 also allow exploring, even if only partially, the uncertainties associated with the modelling assumptions  
536 (e.g., MAT vs WA-PLS, the number of analogues, type metric used to compare pollen samples).

537 The significance tests sensu Telford and Birks (2011) revealed a rather low percentage of  
538 reconstructions to be substantial ( $p < 0.1$ ). However, a failed significance test does not necessarily mean  
539 that the reconstruction is not reliable, but the results should be treated more cautiously, as the Telford-  
540 Birks test is rather conservative (Luoto et al., 2014; Hébert et al., 2022). Several reasons of possible  
541 false negative errors are reported and discussed in the literature, including the test being supposed to  
542 be sensitive to the size of the training data, a low magnitude of an input climate signal, the trajectory of  
543 the core samples through calibration space, or poor analog situations (Luoto et al., 2014; Self et al.,  
544 2015; Andrén et al., 2015, Hébert et al., 2022).

545 All reconstruction methods used in this study heavily rely on extensive collections of modern  
546 assemblage data covering diverse climatic and environmental gradients and are applicable on a broad  
547 spatial scale. As discussed, all the methods may struggle with some intrinsic characteristics of pollen  
548 data and of pollen compilations, including complex species responses, sensitivity to spatial  
549 autocorrelation, limited analogues that may produce poor results in so-called “quantification deserts”  
550 (Chevalier, 2019), where fossil pollen is hardly preserved or nearby modern surface pollen samples are

551 missing (Chevalier et al., 2020). However, we designed our datasets so that more methods can be  
552 included in our reconstruction scripts (<https://doi.org/10.5281/zenodo.5910989>; Herzs Schuh et al.,  
553 2022b), such as CREST, an approach that combines presence-only occurrence data from species  
554 distribution databases instead of modern pollen samples to estimate the responses of pollen taxa to the  
555 climate variable to reconstruct to a climate variable (Chevalier et al., 2014; Chevalier, 2022). CREST is,  
556 therefore, more independent from the availability of modern pollen samples. Employing the Inverse-  
557 Modelling through iterative forward modeling (IMIFM) (Izumi and Bartlein, 2016) might also be possible  
558 in such regions. Its use would be particularly interesting to reconstruct the LGM samples, because  
559 IMIFM is the only technique that can explicitly take the effect of CO<sub>2</sub> on plants (Chevalier et al., 2020).  
560 The inclusion of CREST and/or IMIFM in such large-scale studies would complement our multi-model  
561 reconstruction ensemble by exploring a larger fraction of the “method uncertainty” space in greater  
562 details (e.g. Brewer et al, 2008). Kucera et al. (2005) propose several metrics for a multi-technique  
563 approach to assess the uncertainty space: correlations between the residuals (observed minus  
564 reconstructed values) between pairs of techniques are used to investigate the similarity in the  
565 reconstructions among different techniques. The correlation between the residuals in seasonal  
566 reconstructions (e.g. summer and winter temperatures, summer and annual temperatures) can be used  
567 to investigate the degree of independence of different seasonal reconstructions. Error rate estimates  
568 (RMSEP) determined by cross validation of the calibration data sets and the leaving-one-out method  
569 can be used to compare the calibration of individual transfer function techniques, though it should be  
570 considered that error estimates may vary with the choice of the cross-validation procedure (Kucera et  
571 al., 2005).

572

#### 573 **5.4 Potential use of LegacyClimate 1.0**

574 Our LegacyPollen 1.0 fossil pollen synthesis (Herzs Schuh et al., 2022c) contains records from all over  
575 the Northern Hemisphere extratropics. We used this synthesis to produce our LegacyClimate 1.0  
576 reconstruction data set, which thus can be used to infer spatio-temporal patterns in climate  
577 reconstructions that are not only limited to a local or regional scale. Although several hemispheric or  
578 global reconstruction studies exist, they have been largely restricted to temperature or have included  
579 relatively few records (Marcott et al., 2013; Marsicek et al., 2018; Routson et al., 2019; Kaufman et al.,  
580 2020a and 2020b). Our dataset is therefore a valuable addition. It may be used in a multi-proxy

581 approach, synthesizing marine and terrestrial records in order to assess temperature development  
582 during the Holocene and can help to highlight possible interdependencies between oceans and land  
583 masses. Globally or hemispherically averaged temperature reconstructions from proxy data indicate  
584 peak temperatures during the Holocene Thermal Maximum around 6000 years BP followed by a  
585 pronounced cooling trend toward the late Holocene, which is also visible in our pollen-based  
586 reconstructions (Fig. 10). Hence, spatial variability in the Holocene temperature trends (e.g. missing of  
587 a pronounced maximum for certain latitudinal bands; delayed thermal maximum on land compared to  
588 the ocean) indicate a more local rather than a global Holocene Thermal Maximum (Kaufman et al.,  
589 2020b; Osman et al., 2021; Cartapanis et al., 2022). In contrast, climate models simulate a monotonic  
590 warming throughout the Holocene, which resulted in the “Holocene conundrum” debate (Liu et al., 2014).  
591 The debate has since progressed and hints to discrepancies in data-model comparisons due to  
592 spatiotemporal dynamics related to heterogeneous responses to climate forcing and feedbacks (i.e. the  
593 timing of a Holocene Thermal Maximum in the Northern Hemisphere extra-tropics between  
594 reconstructions from continental and from marine proxy records; Cartapanis et al., 2022) and sometimes  
595 poor spatial averaging due to unevenly distributed proxies. Proxy-only reconstructions often rely on  
596 latitudinal binning and weighting, which makes this approach particularly sensitive to latitudinal bands  
597 that contain only sparse spatial coverage and thus do not represent a true global average (Osman et  
598 al., 2021). Those spatiotemporal dynamics should be considered in data-model comparison.

599 Temperature reconstructions often use either mean annual temperatures (Birks, 2019; Bova et al., 2021)  
600 or global mean surface temperatures (Marcott et al., 2013; Marsicek et al., 2018; Kaufman et al., 2020a  
601 and 2020b). Despite  $T_{\text{ann}}$  being more commonly used in multi-proxy comparisons, it might be useful to  
602 also consider  $T_{\text{July}}$ , as on a regional scale the mean July temperature (or in general summer temperature)  
603 is more important in particular in high latitudes. However, it is argued that proxy-based climate  
604 reconstructions are seasonally biased and therefore might be the reason for the observed proxy-model  
605 divergence (Liu et al., 2014; Rehfeld et al., 2016; Kaufman et al., 2020b). In this respect, it might help  
606 that we provide  $T_{\text{July}}$  along with  $T_{\text{ann}}$  reconstructions derived from our tailoring approach, which provides  
607 the opportunity to assess seasonal impacts on the reconstruction (especially in the high latitudes) in  
608 addition to a consistent reconstruction synthesis.

609 So far, reconstructions of precipitation have not been implemented on a hemispheric scale. The  
610 interconnection between temperature and precipitation (Trenberth, 2011) and its spatio-temporal



611 variation across the Northern Hemisphere is therefore an important aspect of evaluating climate models  
612 (Wu et al., 2013; Hao et al., 2019; Herzschuh et al., 2022a). A broad-scale quantitative reconstruction  
613 of temperature and precipitation would therefore be of great value for evaluating transient climate model  
614 experiments such as TraCE 21k (He, 2010).

615

## 616 **6 Data and code availability**

617 The compilation of reconstructed  $T_{\text{July}}$ ,  $T_{\text{ann}}$ , and  $P_{\text{ann}}$ , is open access and available at PANGAEA  
618 (<https://doi.pangaea.de/10.1594/PANGAEA.930512>; in the “*Other version*” section; Herzschuh et al.,  
619 2021). The dataset files are stored in machine-readable data format (.CSV), which are already separated  
620 into Western North America, Eastern North America, Europe, and Asia for easy access and use.

621 The R code to run the reconstructions for single sites is available at Zenodo  
622 (<https://doi.org/10.5281/zenodo.5910989>; Herzschuh et al., 2022b) including harmonized open-access  
623 modern and fossil pollen datasets so that customized reconstructions can be easily established.

624

625

626

627

628

629

630

631

632

633

634

635

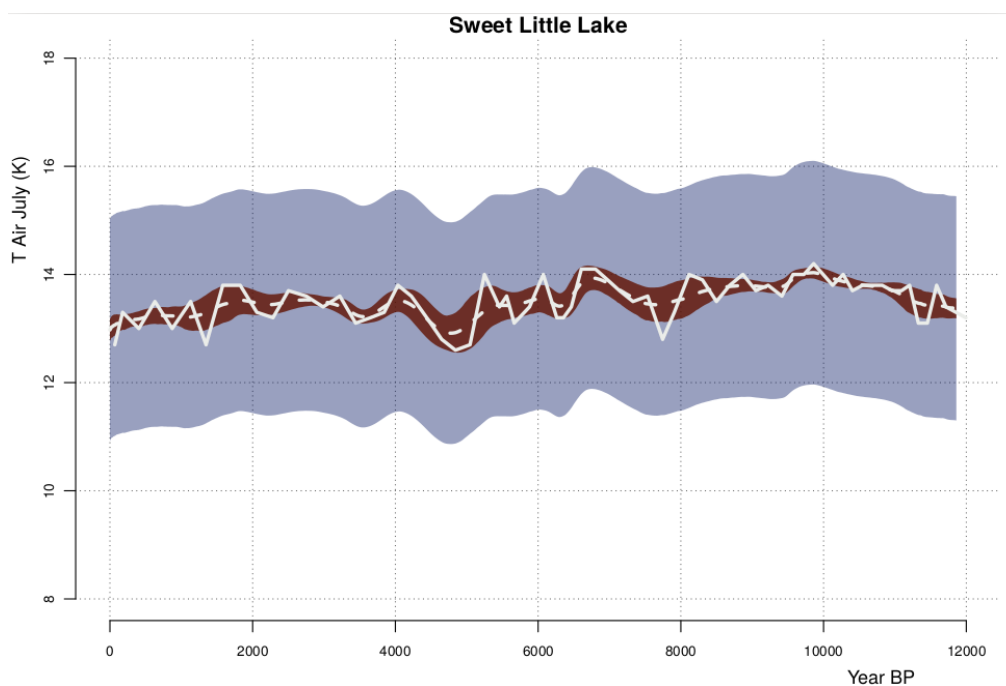
636

637

638

639

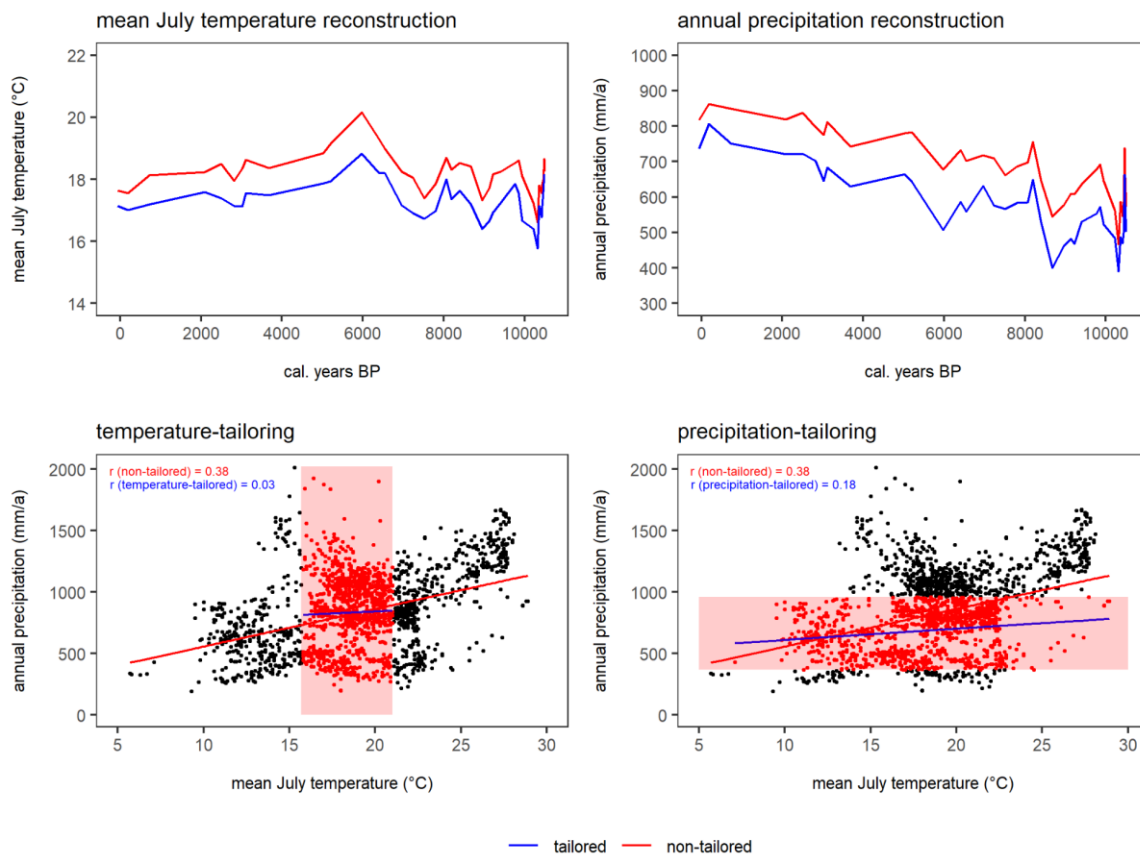
640

641 **Appendix Figures**

642

643 **Appendix Figure 1.** Reconstruction error (shaded blue) and the chronological error (shaded red) around  
644 the reconstruction smoothed by the time-uncertainty (i.e. when we interpolate at regular timesteps for  
645 the 1000 realizations and average over the ensemble, dashed white). The original reconstruction with  
646 the median ages is also shown for comparison (solid white); this underlines that averaging over the age  
647 models only preserves the low-frequencies but (unrealistically) smooths out the high-frequencies.

648



649

650 **Appendix Figure 2.** Example to illustrate the effect of tailoring the modern dataset for the location  
 651 “Yellow Dog Pond” in Eastern North America. Upper part: reconstruction of  $T_{\text{July}}$  and  $P_{\text{ann}}$  with WA-PLS  
 652 (red) and WA-PLS\_tailored (blue); lower part: correlation of  $T_{\text{July}}$  and  $P_{\text{ann}}$  in the modern dataset and the  
 653 effect of tailoring the modern dataset (indicated with the red box). Correlations are given for non-tailored  
 654 (red) and tailored (blue) data.

655

656 **Author contributions.** UH designed the study design and reconstruction dataset. CL and TB compiled  
 657 the metadata and the harmonized pollen dataset. TB wrote the R scripts and ran the analyses under the  
 658 supervision of UH. UH, TB and MC wrote the first draft of the manuscript. All authors discussed the  
 659 results and contributed to the final manuscript.

660 **Competing interests.** The contact author has declared that none of the authors has any competing  
 661 interests.

662 **Acknowledgements.** We would like to express our gratitude to all the palynologists and geologists who,  
 663 either directly or indirectly by providing their work the Neotoma Paleocology Database, contributed

664 pollen data and chronologies to the dataset. The work of data contributors, data stewards, and the  
665 Neotoma community is gratefully acknowledged. We thank Andrej Andreev, Mareike Wieczorek, and  
666 Birgit Heim from AWI for providing information on pollen records and data uploads. We also thank Cathy  
667 Jenks for language editing on a previous version of the paper.

668 **Financial support.** This research has been supported by the European Research Council (ERC Glacial  
669 Legacy 772852 to UH) and the PalMod Initiative (01LP1510C to UH). TB and MC are supported by the  
670 German Federal Ministry of Education and Research (BMBF) as a Research for Sustainability initiative  
671 (FONA; <https://www.fona.de/en>) through the PalMod Phase II project (grant no. FKZ: 01LP1926D). CL  
672 holds a scholarship from the Chinese Scholarship Council (grant no. 201908130165). NR work was  
673 supported by the Russian Science Foundation (Grant No. 20-17-00110).

674

## 675 **References**

676 Andrén, E., Klimaschewski, A., Self, A. E., St. Amour, N., Andreev, A. A., Bennett, K. D., Conley, D.  
677 J., Edwards, T. W. D., Solovieva, N., and Hammarlund, D.: Holocene climate and environmental  
678 change in north-eastern Kamchatka (Russian Far East), inferred from a multi-proxy study of lake  
679 sediments, *Global and Planetary Change*, 134, 41–54,  
680 <https://doi.org/10.1016/j.gloplacha.2015.02.013>, 2015.

681 Behre, K. E.: The rôle of man in European vegetation history. In: Huntley, B., Webb, T. (eds)  
682 *Vegetation history. Handbook of vegetation science*, vol 7. Springer, Dordrecht.  
683 [https://doi.org/10.1007/978-94-009-3081-0\\_17](https://doi.org/10.1007/978-94-009-3081-0_17), 1988.

684 Birks, H. J. B.: Contributions of Quaternary botany to modern ecology and biogeography, *Plant Ecol.*  
685 *Divers.*, 12, 189–385, <https://doi.org/10.1080/17550874.2019.1646831>, 2019.

686 Birks, H. J. B., Heiri, O., Seppä, H., and Bjune, A. E.: Strengths and Weaknesses of Quantitative  
687 Climate Reconstructions Based on Late-Quaternary, *Open Ecol. J.*, 3, 68–110,  
688 <http://dx.doi.org/10.2174/1874213001003020068>, 2010.

689 Blaauw, M. and Christen, J. A.: Flexible paleoclimate age-depth models using an autoregressive  
690 gamma process, *Bayesian Anal.*, 6, 457–474, <https://doi.org/10.1214/11-BA618>, 2011.

- 691 Blois, J. L., Williams, J. W., Grimm, E. C., Jackson, S. T., and Graham, R. W.: A methodological  
692 framework for assessing and reducing temporal uncertainty in paleovegetation mapping from late-  
693 Quaternary pollen records, *Quat. Sci. Rev.*, 30, 1926–1939,  
694 <https://doi.org/10.1016/j.quascirev.2011.04.017>, 2011.
- 695 Bova, S., Rosenthal, Y., Liu, Z., Godad, S. P., and Yan, M.: Seasonal origin of the thermal maxima at  
696 the Holocene and the last interglacial, *Nature*, 589, 548–553, [https://doi.org/10.1038/s41586-020-](https://doi.org/10.1038/s41586-020-03155-x)  
697 [03155-x](https://doi.org/10.1038/s41586-020-03155-x), 2021.
- 698 Brewer, S., Guiot, J., Sánchez-Goñi, M. F., and Klotz, S.: The climate in Europe during the Eemian:  
699 a multi-method approach using pollen data, *Quaternary Science Reviews*, 27, 2303–2315,  
700 <https://doi.org/10.1016/j.quascirev.2008.08.029>, 2008.
- 701 Cao, X., Ni, J., Herzschuh, U., Wang, Y., and Zhao, Y.: A late Quaternary pollen dataset from eastern  
702 continental Asia for vegetation and climate reconstructions: Set up and evaluation, *Rev. Palaeobot.*  
703 *Palynol.*, 194, 21–37, <https://doi.org/10.1016/j.revpalbo.2013.02.003>, 2013.
- 704 Cao, X., Herzschuh, U., Telford, R. J., and Ni, J.: A modern pollen–climate dataset from China and  
705 Mongolia: Assessing its potential for climate reconstruction, *Rev. Palaeobot. Palynol.*, 211, 87–96,  
706 <https://doi.org/10.1016/j.revpalbo.2014.08.007>, 2014.
- 707 Cao, X., Tian, F., Telford, R. J., Ni, J., Xu, Q., Chen, F., Liu, X., Stebich, M., Zhao, Y., Herzschuh, U.,:  
708 Impacts of the spatial extent of pollen-climate calibration-set on the absolute values, range and  
709 trends of reconstructed Holocene precipitation. *Quaternary Science Reviews* 178, 37-53.  
710 <https://doi.org/10.1016/j.quascirev.2017.10.030>, 2017.
- 711 Cao, X., Tian, F., Andreev, A., Anderson, P. M., Lozhkin, A. V., Bezrukova, E., Ni, J., Rudaya, N.,  
712 Stobbe, A., Wiczorek, M., and Herzschuh, U.: A taxonomically harmonized and temporally  
713 standardized fossil pollen dataset from Siberia covering the last 40 kyr, *Earth Syst. Sci. Data*, 12,  
714 119–135, <https://doi.org/10.5194/essd-12-119-2020>, 2020.
- 715 Cartapanis, O., Jonkers, L., Moffa-Sanchez, P., Jaccard, S. L., and de Vernal, A.: Complex spatio-  
716 temporal structure of the Holocene Thermal Maximum, *Nat Commun*, 13, 5662,  
717 <https://doi.org/10.1038/s41467-022-33362-1>, 2022.

- 718 Chen, F., Chen, J., Huang, W., Chen, S., Huang, X., Jin, L., Jia, J., Zhang, X., An, C., Zhang, J., Zhao,  
719 Y., Yu, Z., Zhang, R., Liu, J., Zhou, A., and Feng, S.: Westerlies Asia and monsoonal Asia:  
720 Spatiotemporal differences in climate change and possible mechanisms on decadal to sub-orbital  
721 timescales, *Earth Sci. Rev.*, 192, 337–354, <https://doi.org/10.1016/j.earscirev.2019.03.005>, 2019.
- 722 Chevalier, M.: Enabling possibilities to quantify past climate from fossil assemblages at a global scale,  
723 *Glob. Planet. Change*, 175, 27–35, <https://doi.org/10.1016/j.gloplacha.2019.01.016>, 2019.
- 724 Chevalier, M.: *crestr*: an R package to perform probabilistic climate reconstructions from  
725 palaeoecological datasets, *Clim. Past*, 18, 821–844, <https://doi.org/10.5194/cp-18-821-2022>, 2022.
- 726 Chevalier, M., Cheddadi, R., and Chase, B. M.: CREST (Climate REconstruction SofTware): a  
727 probability density function (PDF)-based quantitative climate reconstruction method, *Clim. Past*, 10,  
728 2081–2098, <https://doi.org/10.5194/cp-10-2081-2014>, 2014.
- 729 Chevalier, M., Davis, B. A. S., Heiri, O., Seppä, H., Chase, B. M., Gajewski, K., Lacourse, T., Telford,  
730 R. J., Finsinger, W., Guiot, J., Köhl, N., Maezumi, S. Y., Tipton, J. R., Carter, V. A., Brussel, T.,  
731 Phelps, L. N., Dawson, A., Zanon, M., Vallé, F., Nolan, C., Mauri, A., de Vernal, A., Izumi, K.,  
732 Holmström, L., Marsicek, J., Goring, S., Sommer, P. S., Chaput, M., and Kupriyanov, D.: Pollen-  
733 based climate reconstruction techniques for late Quaternary studies, *Earth Sci. Rev.*, 210, 103384,  
734 <https://doi.org/10.1016/j.earscirev.2020.103384>, 2020.
- 735 Davis, B. A. S., Zanon, M., Collins, P., Mauri, A., Bakker, J., Barboni, D., Barthelmes, A., Beaudouin,  
736 C., Bjune, A. E., Bozilova, E., Bradshaw, R. H. W., Brayshay, B. A., Brewer, S., Brugiapaglia, E.,  
737 Bunting, J., Connor, S. E., de Beaulieu, J.-L., Edwards, K., Ejarque, A., Fall, P., Florenzano, A.,  
738 Fyfe, R., Galop, D., Giardini, M., Giesecke, T., Grant, M. J., Guiot, J., Jahns, S., Jankovská, V.,  
739 Juggins, S., Kahrman, M., Karpińska-Kołaczek, M., Kołaczek, P., Köhl, N., Kuneš, P., Lapteva, E.  
740 G., Leroy, S. A. G., Leydet, M., Guiot, J., Jahns, S., Jankovská, V., Juggins, S., Kahrman, M.,  
741 Karpińska-Kołaczek, M., Kołaczek, P., Köhl, N., Kuneš, P., Lapteva, E. G., Leroy, S. A. G., Leydet,  
742 M., López Sáez, J. A., Masi, A., Matthias, I., Mazier, F., Meltsov, V., Mercuri, A. M., Miras, Y.,  
743 Mitchell, F. J. G., Morris, J. L., Naughton, F., Nielsen, A. B., Novenko, E., Odgaard, B., Ortu, E.,  
744 Overballe-Petersen, M. V., Pardoe, H. S., Peglar, S. M., Pidek, I. A., Sadori, L., Seppä, H.,  
745 Severova, E., Shaw, H., Święta-Musznicka, J., Theuerkauf, M., Tonkov, S., Veski, S., van der

- 746 Knaap, W. O., van Leeuwen, J. F. N., Woodbridge, J., Zimny, M., and Kaplan, J. O.: The European  
747 Modern Pollen Database (EMPD) project, *Veg. Hist. Archaeobot.*, 22, 521–530,  
748 <https://doi.org/10.1007/s00334-012-0388-5>, 2013.
- 749 Davis, B. A. S., Chevalier, M., Sommer, P., Carter, V. A., Finsinger, W., Mauri, A., Phelps, L. N.,  
750 Zanon, M., Abegglen, R., Åkesson, C. M., Alba-Sánchez, F., Anderson, R. S., Antipina, T. G.,  
751 Atanassova, J. R., Beer, R., Belyanina, N. I., Blyakharchuk, T. A., Borisova, O. K., Bozilova, E.,  
752 Bukreeva, G., Bunting, M. J., Clò, E., Colombaroli, D., Combourieu-Nebout, N., Desprat, S., Di Rita,  
753 F., Djamali, M., Edwards, K. J., Fall, P. L., Feurdean, A., Fletcher, W., Florenzano, A., Furlanetto,  
754 G., Gaceur, E., Galimov, A. T., Gałka, M., García-Moreiras, I., Giesecke, T., Grindean, R., Guido,  
755 M. A., Gvozdeva, I. G., Herzschuh, U., Hjelle, K. L., Ivanov, S., Jahns, S., Jankovska, V., Jiménez-  
756 Moreno, G., Karpińska-Kołaczek, M., Kitaba, I., Kołaczek, P., Lapteva, E. G., Latałowa, M.,  
757 Lebreton, V., Leroy, S., Leydet, M., Lopatina, D. A., López-Sáez, J. A., Lotter, A. F., Magri, D.,  
758 Marinova, E., Matthias, I., Mavridou, A., Mercuri, A. M., Mesa-Fernández, J. M., Mikishin, Y. A.,  
759 Milecka, K., Montanari, C., Morales-Molino, C., Mrotzek, A., Muñoz Sobrino, C., Naidina, O. D.,  
760 Nakagawa, T., Nielsen, A. B., Novenko, E. Y., Panajiotidis, S., Panova, N. K., Papadopoulou, M.,  
761 Pardoe, H. S., Pędziszewska, A., Petrenko, T. I., Ramos-Román, M. J., Ravazzi, C., Rösch, M.,  
762 Ryabogina, N., Sabariego Ruiz, S., Salonen, J. S., Sapelko, T. V., Schofield, J. E., Seppä, H.,  
763 Shumilovskikh, L., Stivrins, N., Stojakowits, P., Svobodova Svitavska, H., Święta-Musznicka, J.,  
764 Tantau, I., Tinner, W., Tobolski, K., Tonkov, S., Tsakiridou, M., et al.: The Eurasian Modern Pollen  
765 Database (EMPD), version 2, *Earth Syst. Sci. Data*, 12, 2423–2445, [https://doi.org/10.5194/essd-](https://doi.org/10.5194/essd-12-2423-2020)  
766 [12-2423-2020](https://doi.org/10.5194/essd-12-2423-2020), 2020.
- 767 Eyring, V., Cox, P. M., Flato, G. M., Gleckler, P. J., Abramowitz, G., Caldwell, P., Collins, W. D., Gier,  
768 B. K., Hall, A. D., Hoffman, F. M., Hurtt, G. C., Jahn, A., Jones, C. D., Klein, S. A., Krasting, J. P.,  
769 Kwiatkowski, L., Lorenz, R., Maloney, E., Meehl, G. A., Pendergrass, A. G., Pincus, R., Ruane, A.  
770 C., Russell, J. L., Sanderson, B. M., Santer, B. D., Sherwood, S. C., Simpson, I. R., Stouffer, R. J.,  
771 and Williamson, M. S.: Taking climate model evaluation to the next level, *Nat. Clim. Chang.*, 9, 102–  
772 110, <https://doi.org/10.1038/s41558-018-0355-y>, 2019.
- 773 Fick, S. E. and Hijmans, R. J.: WorldClim 2: new 1-km spatial resolution climate surfaces for global  
774 land areas, *Int. J. Climatol.*, 37, 4302–4315, <https://doi.org/10.1002/joc.5086>, 2017.

- 775 Gajewski, K., Vance, R., Sawada, M., Fung, I., Gignac, L. D., Halsey, L., John, J., Maisongrande, P.,  
776 Mandell, P., Mudie, P. J., Richard, P. J. H., Sherin, A. G., Soroko, J., and Vitt, D. H.: The climate of  
777 North America and adjacent ocean waters ca. 6 ka. *Canadian Journal of Earth Sciences* 37.5: 661-  
778 681, 2000.
- 779 Hao, Z., Phillips, T. J., Hao, F., and Wu, X.: Changes in the dependence between global precipitation  
780 and temperature from observations and model simulations, *Int. J. Climatol.*, 39, 4895–4906,  
781 <https://doi.org/10.1002/joc.6111>, 2019.
- 782 He, F.: Simulating transient climate evolution of the last deglaciation with CCSM3, Ph.D. thesis,  
783 University of Wisconsin-Madison, USA, 185 pp., 2010.
- 784 Hébert, R., Herzschuh, U., and Laepple, T.: Millennial-scale climate variability over land overprinted  
785 by ocean temperature fluctuations, *Nat. Geosci.*, 15, 899–905, [https://doi.org/10.1038/s41561-022-](https://doi.org/10.1038/s41561-022-01056-4)  
786 01056-4, 2022.
- 787 Herzschuh, U., Cao, X., Laepple, T., Dallmeyer, A., Telford, R. J., Ni, J., Chen, F., Kong, Z., Liu, G.,  
788 Liu, K.-B., Liu, X., Stebich, M., Tang, L., Tian, F., Wang, Y., Wischnewski, J., Xu, Q., Yan, S., Yang,  
789 Z., Yu, G., Zhang, Y., Zhao, Y., and Zheng, Z.: Position and orientation of the westerly jet  
790 determined Holocene rainfall patterns in China, *Nat. Commun.*, 10, 2376,  
791 <https://doi.org/10.1038/s41467-019-09866-8>, 2019.
- 792 Herzschuh, U., Böhmer, T., Li, C., and Cao, X.: Northern Hemisphere temperature and precipitation  
793 reconstruction from taxonomically harmonized pollen data set with revised chronologies using WA-  
794 PLS and MAT (LegacyClimate 1.0), PANGAEA,  
795 <https://doi.pangaea.de/10.1594/PANGAEA.930512>, 2021.
- 796 Herzschuh, U., Böhmer, T., Li, C., Cao, X., Hébert, R., Dallmeyer, A., Telford, R. J., Kruse, S.:  
797 Reversals in temperature-precipitation correlations in the Northern Hemisphere extratropics during  
798 the Holocene. *Geophysical Research Letters*, p.e2022GL099730,  
799 <https://doi.org/10.1029/2022GL099730>, 2022a.
- 800 Herzschuh, U., Böhmer, T., Li, C., Chevalier, M., Dallmeyer, A., Cao, X., Bigelow, N. H., Nazarova,  
801 L., Novenko, E. Y., Park, J., Peyron, O., Rudaya, N. A., Schlütz, F., Shumilovskikh, L. S., Tarasov,



- 802 P. E., Wang, Y., Wen, R., Xu, Q., and Zheng, Z.: LegacyClimate 1.0: A dataset of pollen-based  
803 climate reconstructions from 2594 Northern Hemisphere sites covering the late Quaternary [Data  
804 set], Zenodo, <https://doi.org/10.5281/zenodo.5910989>, 2022b.
- 805 Herzs Schuh, U., Li, C., Böhmer, T., Postl, A. K., Heim, B., Andreev, A. A., Cao, X., Wiczorek, M., and  
806 Ni, J.: LegacyPollen 1.0: a taxonomically harmonized global late Quaternary pollen dataset of 2831  
807 records with standardized chronologies, *Earth Syst. Sci. Data*, 14, 3213–3227,  
808 <https://doi.org/10.5194/essd-14-3213-2022>, 2022c.
- 809 Hijmans, R. J., van Etten, J., Sumner, M., Cheng, J., Baston, D., Bevan, A., Bivand, R., Busetto, L.,  
810 Canty, M., Fasoli, B., Forrest, D., Ghosh, A., Golicher, D., Gray, J., Greenberg, J. A., Hiemstra, P.,  
811 Hingee, K., Ilich, A., Institute for Mathematics Applied Geosciences, Karney, C., Mattiuzzi, M.,  
812 Mosher, S., Naimi, B., Nowosad, J., Pebesma, E., Lamigueiro, O. P., Racine, E. B., Rowlingson,  
813 B., Shortridge, A., Venables, B., and Wueest, R.: Raster: Geographic Data Analysis and Modeling,  
814 R package version 3.5-11, <https://cran.r-project.org/web/packages/raster>, 2021.
- 815 Hill, M. O.: Diversity and Evenness: A Unifying Notation and Its Consequences, *Ecology*, 54, 427–  
816 432, <https://doi.org/10.2307/1934352>, 1973.
- 817 Izumi, K. and Bartlein, P. J.: North American paleoclimate reconstructions for the Last Glacial  
818 Maximum using an inverse modeling through iterative forward modeling approach applied to pollen  
819 data: Pollen-Based Climate Reconstruction, *Geophys. Res. Lett.*, 43, 10,965-10,972,  
820 <https://doi.org/10.1002/2016GL070152>, 2016.
- 821 Jackson, S. T.: Pollen source area and representation in small lakes of the northeastern United States,  
822 *Rev. Palaeobot. Palynol.*, 63, 53–76, [https://doi.org/10.1016/0034-6667\(90\)90006-5](https://doi.org/10.1016/0034-6667(90)90006-5), 1990.
- 823 Jackson, S. T. and Williams, J. W.: MODERN ANALOGS IN QUATERNARY PALEOECOLOGY: Here  
824 Today, Gone Yesterday, Gone Tomorrow?, *Annu. Rev. Earth Planet. Sci.*, 32, 495–537,  
825 <https://doi.org/10.1146/annurev.earth.32.101802.120435>, 2004.
- 826 Juggins, S.: Quantitative reconstructions in palaeolimnology: new paradigm or sick science?,  
827 *Quaternary Science Reviews*, 64, 20–32, <https://doi.org/10.1016/j.quascirev.2012.12.014>, 2013.

- 828 Juggins, S.: rioja: Analysis of Quaternary Science Data, R package version 0.9-21, [https://cran.r-](https://cran.r-project.org/web/packages/rioja)  
829 [project.org/web/packages/rioja](https://cran.r-project.org/web/packages/rioja), 2019.
- 830 Kaufman, D., McKay, N., Routson, C., Erb, M., Davis, B., Heiri, O., Jaccard, S., Tierney, J., Dätwyler,  
831 C., Axford, Y., Brussel, T., Cartapanis, O., Chase, B., Dawson, A., de Vernal, A., Engels, S.,  
832 Jonkers, L., Marsicek, J., Moffa-Sánchez, P., Morrill, C., Orsi, A., Rehfeld, K., Saunders, K.,  
833 Sommer, P. S., Thomas, E., Tonello, M., Tóth, M., Vachula, R., Andreev, A., Bertrand, S.,  
834 Biskaborn, B., Bringué, M., Brooks, S., Caniupán, M., Chevalier, M., Cwynar, L., Emile-Geay, J.,  
835 Fegyveresi, J., Feurdean, A., Finsinger, W., Fortin, M.-C., Foster, L., Fox, M., Gajewski, K.,  
836 Grosjean, M., Hausmann, S., Heinrichs, M., Holmes, N., Ilyashuk, B., Ilyashuk, E., Juggins, S.,  
837 Khider, D., Koinig, K., Langdon, P., Larocque-Tobler, I., Li, J., Lotter, A., Luoto, T., Mackay, A.,  
838 Magyari, E., Malevich, S., Mark, B., Massaferró, J., Montade, V., Nazarova, L., Novenko, E., Pařil,  
839 P., Pearson, E., Peros, M., Pienitz, R., Płóciennik, M., Porinchu, D., Potito, A., Rees, A.,  
840 Reinemann, S., Roberts, S., Rolland, N., Salonen, S., Self, A., Seppä, H., Shala, S., St-Jacques,  
841 J.-M., Stenni, B., Syrykh, L., Tarrats, P., Taylor, K., van den Bos, V., Velle, G., Wahl, E., Walker, I.,  
842 Wilmshurst, J., Zhang, E., and Zhilich, S.: A global database of Holocene paleotemperature records,  
843 *Sci. Data*, 7, 115, <https://doi.org/10.1038/s41597-020-0445-3>, 2020a.
- 844 Kaufman, D., McKay, N., Routson, C., Erb, M., Dätwyler, C., Sommer, P. S., Heiri, O., and Davis, B.:  
845 Holocene global mean surface temperature, a multi-method reconstruction approach, *Sci. Data*, 7,  
846 201, <https://doi.org/10.1038/s41597-020-0445-3>, 2020b.
- 847 Kucera, M., Weinelt, M., Kiefer, T., Pflaumann, U., Hayes, A., Weinelt, M., Chen, M.-T., Mix, A. C.,  
848 Barrows, T. T., Cortijo, E., Duprat, J., Juggins, S., and Waelbroeck, C.: Reconstruction of sea-  
849 surface temperatures from assemblages of planktonic foraminifera: multi-technique approach  
850 based on geographically constrained calibration data sets and its application to glacial Atlantic and  
851 Pacific Oceans, *Quaternary Science Reviews*, 24, 951–998,  
852 <https://doi.org/10.1016/j.quascirev.2004.07.014>, 2005.
- 853 Li, C., Postl, A. K., Böhmer, T., Cao, X., Dolman, A. M., and Herzschuh, U.: Harmonized chronologies  
854 of a global late Quaternary pollen dataset (LegacyAge 1.0), *Earth Syst. Sci. Data*, 14, 1331–1343,  
855 <https://doi.org/10.5194/essd-14-1331-2022>, 2022.

- 856 Liu, Z., Zhu, J., Rosenthal, Y., Zhang, X., Otto-Bliesner, B. L., Timmermann, A., Smith, R. S.,  
857 Lohmann, G., Zheng, W., and Timm, O. E.: The Holocene temperature conundrum, *PNAS*, 111,  
858 E3501–E3505, <https://doi.org/10.1073/pnas.1407229111>, 2014.
- 859 Luoto, T. P., Kaukolehto, M., Weckström, J., Korhola, A., and Väliranta, M.: New evidence of warm  
860 early-Holocene summers in subarctic Finland based on an enhanced regional chironomid-based  
861 temperature calibration model, *Quat. res.*, 81, 50–62, <https://doi.org/10.1016/j.yqres.2013.09.010>,  
862 2014.
- 863 Marcott, S. A., Shakun, J. D., Clark, P. U., and Mix, A. C.: A Reconstruction of Regional and Global  
864 Temperature for the Past 11,300 Years, *Science*, 339, 1198–1201,  
865 <https://doi.org/10.1126/science.1228026>, 2013.
- 866 Marsicek, J., Shuman, B. N., Bartlein, P. J., Shafer, S. L., and Brewer, S.: Reconciling divergent trends  
867 and millennial variations in Holocene temperatures, *Nature*, 554, 92–96,  
868 <https://doi.org/10.1038/nature25464>, 2018.
- 869 Mauri, A., Davis, B. A. S., Collins, P. M., and Kaplan, J. O.: The climate of Europe during the Holocene:  
870 a gridded pollen-based reconstruction and its multi-proxy evaluation, *Quat. Sci. Rev.*, 112, 109–  
871 127, <https://doi.org/10.1016/j.quascirev.2015.01.013>, 2015.
- 872 Nychka, D., Furrer, R., Paige, J., Sain, S., Gerber, F., and Iverson, M.: fields: Tools for Spatial Data,  
873 R package version 10.3, <https://cran.r-project.org/web/packages/fields/index.html>, 2020.
- 874 Oksanen, J., Blanchet, F. G., Friendly, M., Kindt, R., Legendre, P., McGlenn, D., Minchin, P. R.,  
875 O'Hara, R. B., Simpson, G. L., Solymos, P., Stevens, M. H. H., Szoecs, E., and Wagner, H.: Vegan:  
876 Community Ecology Package, R package version 2.5-7, [https://cran.r-](https://cran.r-project.org/web/packages/vegan)  
877 [project.org/web/packages/vegan](https://cran.r-project.org/web/packages/vegan), 2020.
- 878 Osman, M. B., Tierney, J. E., Zhu, J., Tardif, R., Hakim, G. J., King, J., and Poulsen, C. J.: Globally  
879 resolved surface temperatures since the Last Glacial Maximum, *Nature*, 599, 239–244,  
880 <https://doi.org/10.1038/s41586-021-03984-4>, 2021.

- 881 Overpeck, J. T., Webb, T., and Prentice, I. C.: Quantitative Interpretation of Fossil Pollen Spectra:  
882 Dissimilarity Coefficients and the Method of Modern Analogs, *Quat. Res.*, 23, 87–108,  
883 [https://doi.org/10.1016/0033-5894\(85\)90074-2](https://doi.org/10.1016/0033-5894(85)90074-2), 1985.
- 884 Parnell, A. C., Haslett, J., Sweeney, J., Doan, T. K., Allen, J. R. M., and Huntley, B.: Joint  
885 palaeoclimate reconstruction from pollen data via forward models and climate histories, *Quaternary*  
886 *Science Reviews*, 151, 111–126, <https://doi.org/10.1016/j.quascirev.2016.09.007>, 2016.
- 887 R Core Team: R: A language and environment for statistical computing, R Foundation for Statistical  
888 Computing, Vienna, Austria, available online at: <https://www.R-project.org/>, 2020.
- 889 Rehfeld, K., Trachsel, M., Telford, R. J., and Laepple, T.: Assessing performance and seasonal bias  
890 of pollen-based climate reconstructions in a perfect model world, *Clim. Past*, 12, 2255–2270,  
891 <https://doi.org/10.5194/cp-12-2255-2016>, 2016.
- 892 Routson, C. C., McKay, N. P., Kaufman, D. S., Erb, M. P., Goosse, H., Shuman, B. N., Rodysill, J. R.,  
893 and Ault, T.: Mid-latitude net precipitation decreased with Arctic warming during the Holocene,  
894 *Nature*, 568, 83–87, <https://doi.org/10.1038/s41586-019-1060-3>, 2019.
- 895 Self, A. E., Jones, V. J., and Brooks, S. J.: Late Holocene environmental change in arctic western  
896 Siberia, *The Holocene*, 25, 150–165, <https://doi.org/10.1177/0959683614556387>, 2015.
- 897 Simpson, G. L.: Analogue Methods in Palaeolimnology, in: *Tracking Environmental Change Using*  
898 *Lake Sediments: Data Handling and Numerical Techniques*, edited by: Birks, H. J. B., Lotter, A. F.,  
899 Juggins, S., and Smol, J. P., Springer Netherlands, Dordrecht, 495–522,  
900 [https://doi.org/10.1007/978-94-007-2745-8\\_15](https://doi.org/10.1007/978-94-007-2745-8_15), 2012.
- 901 Simpson, G. L., Oksanen, J., Maechler, M.: analogue: Analogue and Weighted Averaging Methods  
902 for Palaeoecology, R package version 0.17-6, <https://cran.r-project.org/web/packages/analogue/>,  
903 2021.
- 904 Sugita, S.: A Model of Pollen Source Area for an Entire Lake Surface, *Quat. Res.*, 39, 239–244,  
905 <https://doi.org/10.1006/qres.1993.1027>, 1993.

- 906 Tarasov, P. E., Nakagawa, T., Demske, D., Österle, H., Igarashi, Y., Kitagawa, J., Mokhova, L.,  
907 Bazarova, V., Okuda, M., Gotanda, K., Miyoshi, N., Fujiki, T., Takemura, K., Yonenobu, H., and  
908 Fleck, A.: Progress in the reconstruction of Quaternary climate dynamics in the Northwest Pacific:  
909 A new modern analogue reference dataset and its application to the 430-kyr pollen record from  
910 Lake Biwa, *Earth Sci. Rev.*, 108, 64–79, <https://doi.org/10.1016/j.earscirev.2011.06.002>, 2011.
- 911 Telford, R. J.: palaeoSig: Significance Tests for Palaeoenvironmental Reconstructions, R package  
912 version 2.0-3, <https://cran.r-project.org/web/packages/palaeoSig>, 2019.
- 913 Telford, R. J. and Birks, H. J. B.: A novel method for assessing the statistical significance of  
914 quantitative reconstructions inferred from biotic assemblages, *Quat. Sci. Rev.*, 30, 1272–1278,  
915 <https://doi.org/10.1016/j.quascirev.2011.03.002>, 2011.
- 916 ter Braak, C. J. F.: CANOCO - a FORTRAN program for canonical community ordination by (Partial)  
917 (Detrended) (Canonical) correspondence analysis and redundancy analysis. Agricultural  
918 Mathematics Group, Wageningen, 1988.
- 919 ter Braak, C. J. F. and Juggins, S.: Weighted averaging partial least squares regression (WA-PLS):  
920 an improved method for reconstructing environmental variables from species assemblages,  
921 *Hydrobiologia*, 269, 485–502, <https://doi.org/10.1007/BF00028046>, 1993.
- 922 Tian, F., Cao, X., Dallmeyer, A., Zhao, Y., Ni, J., and Herzschuh, U.: Pollen-climate relationships in  
923 time (9 ka, 6 ka, 0 ka) and space (upland vs. lowland) in eastern continental Asia, *Quat. Sci. Rev.*,  
924 156, 1–11, <https://doi.org/10.1016/j.quascirev.2016.11.027>, 2017.
- 925 Trachsel, M. and Telford, R. J.: All age–depth models are wrong, but are getting better, *Holocene*, 27,  
926 860–869, <https://doi.org/10.1177/0959683616675939>, 2017.
- 927 Trenberth, K. E.: Changes in precipitation with climate change, *Clim. Res.*, 47, 123–138,  
928 <https://doi.org/10.3354/cr00953>, 2011.
- 929 Whitmore, J., Gajewski, K., Sawada, M., Williams, J. W., Shuman, B., Bartlein, P. J., Minckley, T.,  
930 Viau, A. E., Webb, T., Shafer, S., Anderson, P., and Brubaker, L.: Modern pollen data from North  
931 America and Greenland for multi-scale paleoenvironmental applications, *Quat. Sci. Rev.*, 24, 1828–  
932 1848, <https://doi.org/10.1016/j.quascirev.2005.03.005>, 2005.

933 Williams, J. W., Grimm, E. C., Blois, J. L., Charles, D. F., Davis, E. B., Goring, S. J., Graham, R. W.,  
934 Smith, A. J., Anderson, M., Arroyo-Cabrales, J., Ashworth, A. C., Betancourt, J. L., Bills, B. W.,  
935 Booth, R. K., Buckland, P. I., Curry, B. B., Giesecke, T., Jackson, S. T., Latorre, C., Nichols, J.,  
936 Purdum, T., Roth, R. E., Stryker, M., and Takahara, H.: The Neotoma Paleoecology Database, a  
937 multiproxy, international, community-curated data resource, *Quat. Res.*, 89, 156–177,  
938 <https://doi.org/10.1017/qua.2017.105>, 2018.

939 Williams, J. W., Webb III, T., Richard, P. H., and Newby, P.: Late Quaternary biomes of Canada and  
940 the eastern United States, *J. Biogeogr.*, 27, 585–607, [https://doi.org/10.1046/j.1365-](https://doi.org/10.1046/j.1365-2699.2000.00428.x)  
941 [2699.2000.00428.x](https://doi.org/10.1046/j.1365-2699.2000.00428.x), 2000.

942 Wu, R., Chen, J., and Wen, Z.: Precipitation-surface temperature relationship in the IPCC CMIP5  
943 models, *Adv. Atmos. Sci.*, 30, 766–778, <https://doi.org/10.1007/s00376-012-2130-8>, 2013.

944 Zanon, M., Davis, B. A. S., Marquer, L., Brewer, S., and Kaplan, J. O.: European Forest Cover During  
945 the Past 12,000 Years: A Palynological Reconstruction Based on Modern Analogs and Remote  
946 Sensing, *Front. Plant Sci.*, 9, 253, <https://doi.org/10.3389/fpls.2018.00253>, 2018.